LS Scienza dei Materiali - a.a. 2006/07

Fisica delle Nanotecnologie – part 7

Version 5, Dec 2006

Francesco Fuso, tel 0502214305, 0502214293 - fuso@df.unipi.it
http://www.df.unipi.it/~fuso/dida

Confinamento quantico, trasporto elettronico e tunneling in nanostrutture 2-DEG,1-DEG, 0-DEG

15/12/2006 – 14.30-16.30 – room T1

What are we looking for...

We deal with particles (e.g., electrons) moving in nanosized structures

Quantum treatment of the particles implies wavefunctions (e.g., de Broglie,..)

If wavefunction extension ~ structure size, we expect **quantum confinement**

Known examples in **optics** (λ~hundreds of nm): optical cavity, optical fibers
Signatures of quantization: radiation modes, supported standing waves, …

λ_{dB} = h/p ~ 7x10^{-4}/v [m/s] in nm
(v_{term}~10^{4} -10^{5} m/s, v_F~10^{6} m/s)

In **transport properties**, dimensions are scaled down to the de Broglie wavelength, so nanosized structures are needed (contrary to optics, where sum-micron range is typical)
Expected signatures of quantization: non-ohmic behavior, tunneling effects, single electron, …

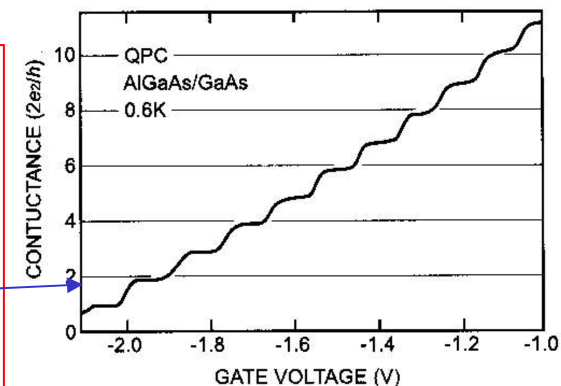

Many potential advantages (in, e.g., electronics):
miniaturization, speed, consumption, *novel functions,…*

Outlook

- Focus on "conventional" (silicon-based, inorganics) technology (we will mention other possibilities later on)

A. Electron transport and quantum confinement in **2-D structures in the presence of a magnetic field**:
   - High mobility 2-D electron gases at heterostructure interface;
   - Quantum electron in a magnetic field: Landau levels;
     - Quantum Hall Effect (integer, and a few words on the fractional effect);
     - von Klitzing quantum of resistance

B. Electron transport and quantum confinement in **1-D structures without magnetic field**:
   - Landauer treatment and levels;
   - electron waveguides: "transverse modes"

C. Electron transport and quantum confinement **through** **0-D structures**:
   - tunneling effects;
   - single electron phenomena and devices

Conductivity in the classical (macroscopic) world

(Microscopic) Ohm's law:
$\mathbf{J} = \sigma \mathbf{E} \rightarrow I = V/R$ with $R = l/(S\,\sigma)$

In classical terms, resistance is a function of the dimensions (in bulk 3D materials, it is directly proportional to the length l and inversely proportional to the cross section S): **R ~ (typical width)^(2-dimensionality)**

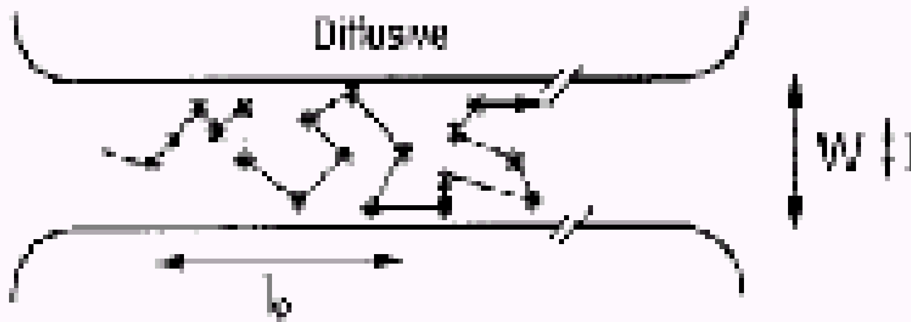

Drude (either classical or quantum):
Diffusional motion of the electrons

"Collisional" processes (material-dependent) rule the resistivity

Dimensionality enters transport properties also in conventional pictures!

Electron transport and quantum confinement

Transport properties depend on the dimensionality of the structures, first of all because of the peculiar density-of-states expression: new and unexpected effects associated with quantum confinement can arise

Quantum confinement is hard to be seen in 2DEG (2-dimension electron gases, e.g., conductive films), since the “macroscopic degrees of freedom” tend to mask any possible quantized effect

Fully localized 0DEG structures (quantum dots) do require other processes for transport tooccurr (e.g., tunneling, as we will see)

Basically, 1DEG structures are well suited for investigating electron transport (quantum wires)

Hystorically, the first observations are associated with the Quantum Hall Effect (QHE) in specific 2DEG structures with the presence of a static magnetic field

2DEG in semiconducting heterostructures

1.1 Two-dimensional electron gas (2-DEG)

Recent work on mesoscopic conductors has largely been based on GaAs–AlGaAs heterojunctions where a thin two-dimensional conducting layer is formed at the interface between GaAs and AlGaAs. To understand why this layer is formed consider the conduction and valence band line-up in the z-direction when we first bring the layers in contact (Fig. 1.1.1a). The Fermi energy E_f in the widegap AlGaAs layer is higher than that in the narrowgap GaAs layer. Consequently electrons spill over from the n-AlGaAs leaving behind positively charged donors. This space charge gives rise to an electrostatic potential that causes the bands to bend as shown. At equilibrium the Fermi energy is constant everywhere. The electron density is sharply peaked near the GaAs–AlGaAs interface (where the Fermi energy is inside the conduction band) forming a thin conducting layer which is usually referred to as the two-dimensional electron gas (2-DEG in short). The carrier concentration in a 2-DEG typically ranges from $2 \times 10^{11}/\mathrm{cm}^2$ to $2 \times 10^{12}/\mathrm{cm}^2$ and can be depleted by applying a negative voltage to a metallic gate deposited on the surface. The practical importance of this structure lies in its use as a field effect transistor [1.2, 1.3] which goes under a variety of names such as MODFET (MOdulation Doped Field Effect Transistor) or HEMT (High Electron Mobility Transistor).

Note that this structure is similar to standard silicon MOSFETs, where the 2-DEG is formed in silicon instead of GaAs. The role of the wide-gap AlGaAs is played by a thermally grown oxide layer (SiO_x). Indeed much of the pioneering work on the properties of two-dimensional conductors was performed using silicon MOSFETs [1.4]

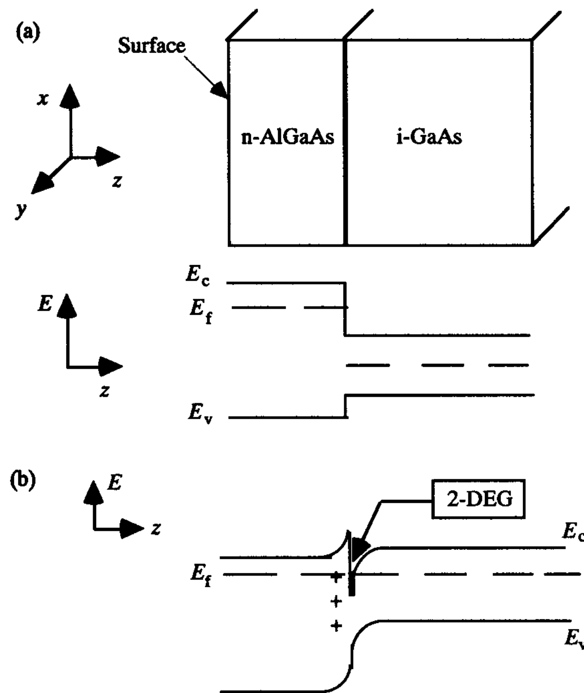

Fig. 1.1.1. Conduction and valence band line-up at a junction between an n-type AlGaAs and intrinsic GaAs, (*a*) before and (*b*) after charge transfer has taken place. Note that this is a cross-sectional view. Patterning (as shown in Fig. 0.3) is done on the surface (*x*–*y* plane) using lithographic techniques.

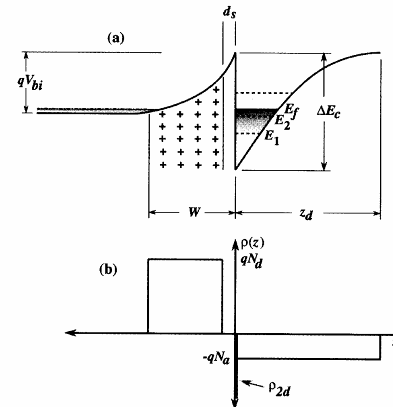

ig. 2.12. (a) Conduction band profile through a modulation-doped heterojunction system. (b) Charge ensity versus distance due to ionized donors and acceptors.

After Ferry and Goodnick, Transport in nanostructures, Cambridge (1997)

After S.Datta, Electronic Transport in Mesoscopic Systems, Cmbridge (1997)

"Band bending" at the interface produces localization in a 2DEG with typ. thickness 1-10 nm

Reminder on Fermi level in doped semiconductors I

Fermi level and carrier density in doped semiconductors

rrier concentration in n-type semiconductors

e consider now extrinsic semiconductors, containing donor impurities, or acceptor npurities, or both, and we wish to study their influence on the Fermi level and e free carrier concentrations. We consider first the case of semiconductors in which nly donor impurities are present (*n-type semiconductors*). The density N_d of donor npurities is supposed to be uniform in the sample, and the binding energy of the onor levels is ε_d. The schematic representation of the energy levels and occupancy at $T = 0$) is given in Fig. 7a.

In intrinsic semiconductors we have seen that the Fermi level lies (basically) at the niddle of the energy gap (see Eq. 6). Doping with donors (or acceptor) levels is the most common method to change in a controlled way the position of the Fermi level within the energy gap. The presence of donor levels shifts the Fermi level from the middle of the energy gap toward the edge of the conduction band. Let us in fact define the temperature

$$k_B T_d \equiv \varepsilon_d \ ,$$

where T_d can be considered as the "ionization temperature" of the donor levels. If $T \ll T_d$ we expect that practically all donor levels are occupied and thus the chemical potential must be located in the energy range $E_d < \mu(T) < E_c$. If T is comparable with T_d we expect that most donor levels are ionized and $\mu(T)$ lies somewhat below the donor energy E_d, but still very near to the conduction band edge. At temperatures so high that the intrinsic carriers are much larger than the concentration of donor impurities, doping becomes uninfluential and we expect that the chemical potential approaches the middle of the bandgap. The chemical potential and the carrier concentration can be determined quantitatively from the knowledge of donor concentration, density-of-states of the bulk crystal, and appropriate Fermi–Dirac statistics for band levels and donor levels.

The impurity states within the energy gap are described by localized wavefunctions; a donor level can thus be empty, or occupied by one electron of either spin, but not by two electrons (of opposite spin) because of the penalty in the electrostatic repulsion energy. Due to this, the probability $P(E_d)$ that the level E_d is occupied by an electron of either spin is given by

$$P(E_d) = \frac{1}{(1/2)\, e^{(E_d-\mu)/k_BT} + 1} \ ; \qquad (19)$$

the above expression has been derived in Appendix III-C in the same way as the fundamental Fermi–Dirac statistics (1).

The chemical potential of the doped semiconductor is determined by enforcing the conservation of the total number of electrons as the temperature changes. In a semiconductor with N_d donor impurities per unit volume, the density $n_0(T)$ of electrons in the conduction band must satisfy the relation

$$\boxed{n_0(T) = N_d\,[1 - P(E_d)] + p_0(T)} \qquad (20)$$

where n_0 and p_0 are given by expressions (2). Eq. (20) is the straightforward generalization of Eq. (3); it states that the free electrons in the conduction bands are supplied by the thermal ionization of donor levels and by the thermal excitation of valence electrons. Eq. (20) can also be interpreted as an overall *charge neutrality condition* in the sample: the concentration n_0 of negative charges equals the concentration of ionized donor impurities plus the concentration of holes.

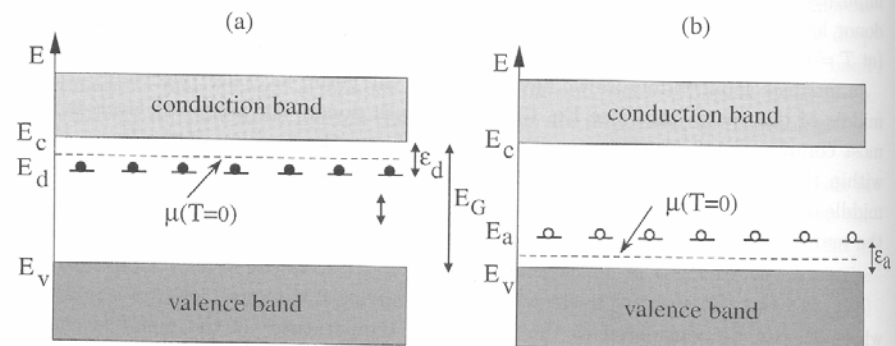

Fig. 7 (a) Schematic representation of the energy levels of a homogeneously doped n-type semiconductor at $T = 0$ (in abscissa any arbitrary direction in the homogeneous material can be considered). Typical energy values are $E_G = E_c - E_v \approx 1\,\text{eV}$ and $\varepsilon_d = E_c - E_d \approx 10\,\text{meV}$. The Fermi level at zero temperature lies at $(1/2)(E_d + E_c)$, which is the middle point between E_d and E_c. (b) Schematic representation of the energy levels of a homogeneously doped p-type semiconductor at $T = 0$; typical values of $\varepsilon_a = E_a - E_v$ are of the order of 10 meV. The Fermi level at zero temperature lies at $(1/2)(E_v + E_a)$, which is the middle point between E_v and E_a.

G.Grosso and G.Pastori Parravicini,
Solid State Physics (Academic, 2000)

Reminder on Fermi level in doped semiconductors II

Equation (20) can be solved (numerically) to obtain the Fermi level and hence the free carrier concentration. In the case the n-type semiconductor is non-degenerate (which is the ordinary situation, except for extremely high concentration of dopants), Eq. (20) can be simplified using Eqs. (5). We have:

$$N_c(T)\, e^{-(E_c-\mu)/k_BT} = N_d \frac{(1/2)\, e^{(E_d-\mu)/k_BT}}{(1/2)\, e^{(E_d-\mu)/k_BT}+1} + N_v(T)\, e^{-(\mu-E_v)/k_BT} \,. \qquad (21)$$

This is a third order algebraic expression in $x = \exp(\mu/k_BT)$ that could be easily solved. We prefer to consider Eq. (21) in different regions of physical interest and handle it analytically.

(i) *Very low temperatures (or "freezing out region").* Consider the semiconductor at very low temperatures $T \ll T_d$. In this temperature region we certainly have

$$E_d < \mu(T) < E_c \,.$$

Thus the second term in the right hand side of Eq. (21) can safely be neglected; furthermore the denominator in the first term in the right-hand side of Eq. (21) can be taken as unity. We have thus

$$N_c(T)\, e^{-(E_c-\mu)/k_BT} = \frac{1}{2} N_d\, e^{(E_d-\mu)/k_BT} \,; \qquad (22a)$$

taking the logarithm of both members we obtain for the Fermi level

Low T

$$\mu(T) = \frac{1}{2}(E_d + E_c) + \frac{1}{2} k_B T \ln \frac{N_d}{2N_c(T)} \,. \qquad (2$$

We can replace expression (22b) into equation (22a), and we obtain that the ca density in the conduction band is

$$n_0(T) = N_c(T)\, e^{-(E_c-\mu)/k_BT} = \sqrt{N_c(T) \frac{N_d}{2}}\, e^{-\varepsilon_d/2k_BT} \,.$$

Thus, the temperature dependence of the free electron carriers in n-type semicon tors at temperatures $T \ll T_d$ has (approximately) the exponential form $\exp(-\Delta/k$ where Δ is *half the binding energy of the donor levels*. Notice that for high do Eq. (22b) shows a tendency of $\mu(T)$ to increase and possibly to invade the conduc band; in this situation we must consider directly the implicit equation (20) for determination of the chemical potential.

(ii) *Saturation region.* Consider the semiconductor in the temperature region T $T \ll E_G/k_B$; we expect that (almost) all donor levels are ionized, while the ther excitation of valence electrons is still negligible. We have

$$n_0(T) = N_c(T)\, e^{-(E_c-\mu)/k_BT} \cong N_d \,; \qquad (2$$

from the logarithm of both members, we have for the chemical potential

Intermediate T

$$\mu(T) = E_c + k_B T \ln \frac{N_d}{N_c(T)} \,. \qquad (2$$

While the number $n_0(T)$ of majority carriers is essentially constant and equal N_d, t number of minority carriers is obtained by considering the mass-action law (7). In t *saturation region*, characterized by all donor levels ionized, and at temperatures wh

$n_i(T) \ll N_d$, we have

$$n_0(T) \cong N_d \quad \text{and} \quad p_0(T) \cong \frac{n_i^2(T)}{N_d} \,. \qquad (24c)$$

For instance, the intrinsic carrier concentration of silicon at room temperature is $n_i(T) \approx 10^{10}\,\mathrm{cm}^{-3}$. In n-type silicon with donor concentration $N_d \approx 10^{14}\,\mathrm{cm}^{-3}$, we have $n_0 \approx 10^{14}\,\mathrm{cm}^{-3}$ and $p_0 \approx 10^6\,\mathrm{cm}^{-3}$; in the above situation there are eight orders of magnitude in the difference between the concentration of majority carriers and of minority carriers. Notice also that in silicon $N_c(T) \approx 10^{19}\,\mathrm{cm}^{-3}$; the chemical potential (24b) remains near the conduction band edge, but safely below it, so that the non-degeneracy conditions (4) are justified. As another example, consider an n-type GaAs crystal at room temperature with $n_i(T) \approx 10^7\,\mathrm{cm}^{-3}$ and $n_0 \approx N_d \approx 10^{14}\,\mathrm{cm}^{-3}$; in this case we have $p_0 \approx 1\,\mathrm{cm}^{-3}$, a value fourteen orders of magnitude less than the majority carrier concentration.

High T

(iii) *Intrinsic region.* If we increase further the temperature, the thermal excitation of valence electrons into the conduction band increases, and eventually the intrinsic situation is recovered. The temperature dependence of the density of free electron carriers in an n-type semiconductor is schematically summarized in Fig. 8.

Up to this point, impurities have been (tacitly) considered as isolated and independent; furthermore the doped semiconductor is assumed to remain non-degenerate, i.e. the Fermi level is several k_BT away from the band edges. As the concentration of dopants is increased new phenomena occur; for instance, the Fermi level may approach and invade the energy bands; the density-of-states of the semiconductor may be perturbed near the edges and a bandgap narrowing may result; the impurity levels may interact forming an impurity band, with effects on the conductivity of the sample; here, we do not enter in these and other interesting consequences of heavy doping in semiconductors.

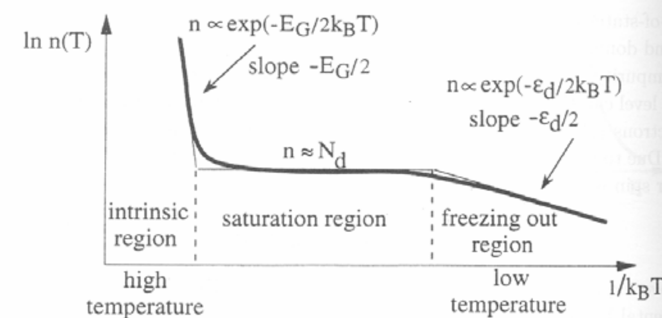

Fig. 8 Schematic variation of the electron concentration as a function of $1/k_BT$ in an n-ty semiconductor with N_d donor impurities per unit volume.

High mobility in MODFET/HEMT structures

Mobility

What makes the 2-DEG in GaAs very special is the extremely low scattering rates that have been achieved. The mobility (at low temperatures) provides a direct measure of the momentum relaxation time as limited by impurities and defects. Let us first briefly explain the meaning of mobility. In equilibrium the conduction electrons move around randomly not producing any current in any direction. An applied electric field **E** gives them a drift velocity $\mathbf{v}_d$ in the direction of the force $e\mathbf{E}$ as shown in Fig. 1.1.2. To relate the drift velocity to the electric field we note that, at steady-state, the rate at which the electrons receive momentum from the external field is exactly equal to the rate at which they lose momentum (**p**) due to scattering forces:

$$\left[\frac{d\mathbf{p}}{dt}\right]_{\text{scattering}} = \left[\frac{d\mathbf{p}}{dt}\right]_{\text{field}}$$

Hence, (τ_m: momentum relaxation time)

$$\frac{m\mathbf{v}_d}{\tau_m} = e\mathbf{E} \quad \Rightarrow \quad \mathbf{v}_d = \frac{e\tau_m}{m}\mathbf{E}$$

The mobility is defined as the ratio of the drift velocity to the electric field:

$$\mu \equiv \left|\frac{v_d}{E}\right| = \frac{|e|\tau_m}{m} \qquad (1.1.1)$$

Mobility measurement using the Hall effect (see Section 1.5) is a basic characterization tool for semiconducting films. Once the mobility is known, the momentum relaxation time is readily deduced from Eq.(1.1.1).

In bulk semiconductors as we go down from room temperature, the momentum relaxation time increases at first due to the suppression of phonon scattering. But it does not increase any further once the phonon scattering is small enough that impurity scattering becomes the dominant mechanism (see Fig. 1.1.3). With a donor concentration of $10^{17}/\text{cm}^3$ the highest mobility is less than 10^4 cm^2/V s. Higher mobilities can be obtained with undoped samples but this is not very useful since there are very few conduction electrons.

In a 2-DEG, on the other hand, carrier concentrations of $10^{12}/\text{cm}^2$ in a layer of thickness ~100 Å (equivalent bulk concentration of $10^{18}/\text{cm}^3$) have been obtained with mobilities in excess of 10^6 cm^2/V s (the current record is almost an order of magnitude larger than what is shown in Fig. 1.1.3). The reason is the spatial separation between the donor atoms in the AlGaAs layer and the conduction electrons in the GaAs layer. This reduces the scattering cross-section due to the impurities, leading to weaker scattering. Often an extra buffer layer of undoped AlGaAs is introduced between the GaAs and the n-AlGaAs in order to increase the separation between the 2-DEG in the GaAs and the ionized donors in the AlGaAs. This reduces the scattering but it also reduces the carrier concentration.

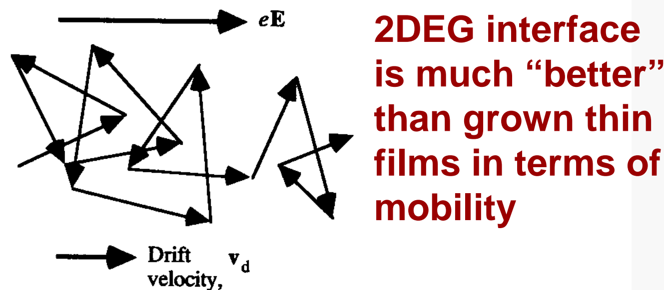

Fig. 1.1.2. In the presence of an electric field the electrons acquire a drift velocity superposed on their random motion.

2DEG interface is much "better" than grown thin films in terms of mobility

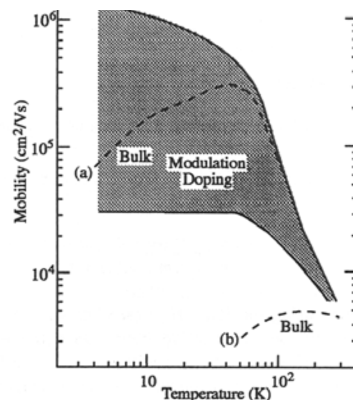

Fig. 1.1.3. Mobility vs. temperature in modulation-doped structures. Higher mobility (but lower carrier concentration) is obtained with thicker buffer layers. Also shown for comparison is the mobility in (a) high purity bulk GaAs and in (b) doped GaAs for use in FETs. Adapted with permission from Fig. 9 of T. J. Drummond, W. T. Masselink and H. Morkoc (1986). *Proc. IEEE*, 74, 779. © 1986 IEEE

High "in-plane" mobility achieved (negligible collision rates)

Classical Hall effect in a conductor

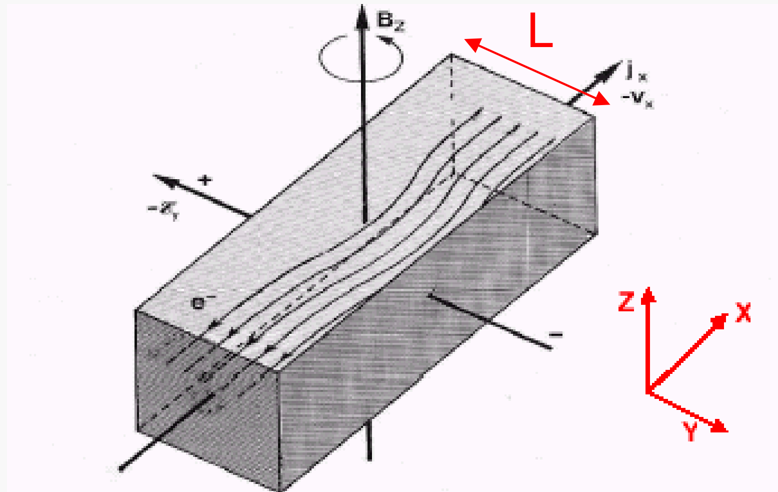

$$V_H = R_H I = v_d B L = \mu B L / e$$

Mobility can be measured (including the sign) by Hall experiments

Classically, the Hall resistance is a continuous (i.e., non-quantized) feature depending on the mobility

A known current is sent along *x*

A known magnetic field (static and homogeneous) is applied along *z*

In a two-charge fluid model of the current, Lorentz force drives positive and negative charge along *y*, with a sign depending on the charge polarity

At equilibrium, charge separation occurs (along *y*)
-> an electric field exists
-> a potential difference can be measured across *y* direction

A. Electron dynamics in a magnetic field (quantum)

Effetti qauntistici: diventano importanti ad esempio quando la separazione dei livelli energetici quantizzati è paragonabile a energia del sistema, oppure quando la lunghezza d'onda di de Broglie $\lambda_{dB} = h/p$ si avvicina ad una lunghezza caratteristica del sistema.

Nel QHE si ha quantizzazione dell'energia dovuta alla presenza di B, che produce effetti osservabili (anche per valori di campo *realistici*) grazie alle piccole dimensioni del sistema in una direzione.

0.1 Moto classico di un elettrone in presenza di B

Suppongo $\mathbf{B} = B\,\hat{z}$. Dalla forza di Lorentz

$$\mathbf{F}_{Lorentz} = -e\mathbf{v} \times \mathbf{B} \qquad (1)$$

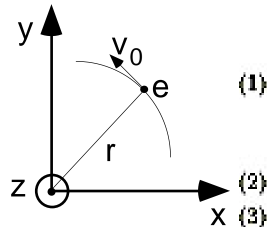

si ha:

$$m\dot{v}_x = -ev_yB \qquad (2)$$
$$m\dot{v}_y = ev_xB\,, \qquad (3)$$

da cui (derivando e sostituendo):

$$m\ddot{v}_x = -\frac{e^2B^2}{m}v_x\,. \qquad (4)$$

Il moto lungo x ed y è oscillatorio con la pulsazione di ciclotrone $\omega_c = eB/m$. La combinazione dei moti lungo x ed y con opportune condizioni iniziali da luogo ad uno moto circolare con la stessa pulsazione e *raggio arbitrario* (purché $\omega_c = v_0/r$). Se l'elettrone ha anche moto lungo z, la traiettoria è una spirale.

0.2 Trattazione quantistica

L'Hamiltoniana di un elettrone in presenza di B è (gauge di Lorentz)*:

$$\mathcal{H} = \frac{1}{2m}(\mathbf{p} - e\mathbf{A})^2\,, \qquad (5)$$

con A potenziale vettore ($\nabla \times \mathbf{A} = \mathbf{B}$). Nel nostro caso conviene scegliere $\mathbf{A} = (-By, 0, 0)$, quindi si ha:

$$\mathcal{H} = \frac{1}{2m}((p_x + eBy)^2 + p_y^2 + p_z^2)\,. \qquad (6)$$

Dato che non compare dipendenza esplicita né da x né da z, p_x e p_z sono costanti del moto, quindi la soluzione sarà del tipo $\psi = \exp(ik_xx)\exp(ik_zz)\mathcal{F}(y)$, con

* $\phi \rightarrow \phi + \frac{\partial\psi}{\partial t}$, $A \rightarrow A - \nabla\psi$, $\quad \frac{1}{c^2}\frac{\partial\phi}{\partial t} + \nabla\cdot A = 0.$

$\mathcal{F}(y)$ funzione da determinare attraverso l'applicazione dell'eq. di Schrödinger (Eq. 6), che dà:

$$-\frac{\hbar^2}{2m}\frac{\partial^2\mathcal{F}}{\partial y^2} + \frac{1}{2}m\omega_c^2(y - y_0)^2\mathcal{F} = E'\mathcal{F}\,, \qquad (7)$$

con E' espressione opportuna di energia. Questa è l'equazione di un oscillatore armonico lungo y con pulsazione ω_c e *centro di oscillazione*:

$$y_0 = -\frac{\hbar k_x}{eB}\,. \qquad (8)$$

I livelli di energia sono quantizzati con autovalori:

$$E_{n,j} = E_{kin} + (n + \frac{1}{2})\hbar\omega_c\,, \qquad (9)$$

dove j è un numero quantico riferito all'energia cinetica E_{kin}. Si noti che i valori del quanto di energia sono genralmente bassi (meV o frazioni di meV) per campi magnetici usuali.

Se il sistema ha piccole dimensioni lungo y (supponiamo lo spessore sia L), allora deve essere $|y_0| \leq L$, da cui:

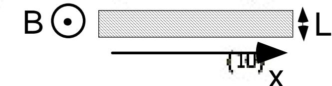

$$k_x < \frac{eBL}{\hbar} = \frac{\omega_c mL}{\hbar}\,. \qquad (10)$$

Quindi, la bassa dimensionalità lungo y produce una limitazione sul valore di k_x (effetto di "mescolamento" delle direzioni spaziali tipico delle situazioni in cui si ha a che fare con un campo magnetico).

0.3 Densità degli stati e degenerazione

Nel caso unidmensionale, che qui si applica per tenere conto del confinamento spaziale lungo la direzione y, e di conseguenza del confinamento nello spazio k lungo la direzione x (vedi Eq. (10)), si ha che la densità degli stati (riferita solo alla direzione di quantizzazione) è:

$$g(k_x)dk_x = dk_x\frac{L}{2\pi}\,. \qquad (11)$$

1-DEG DOS

Considerando la sola direzione x, integrando si ottiene:

$$\int_0^{k} dk_x\frac{L}{2\pi} = \frac{eBL^2}{2\pi\hbar}\,, \qquad (12)$$

dove si è tenuto conto della condizione Eq. (10). Dividendo l'espressione al membro di destra di Eq. (12) per L^2 si ottiene in pratica una densità (n_s) di portatori di carica per unità di superficie (reale), che vale quindi:

$$n_s = \frac{eB}{2\pi\hbar}\,. \qquad (13)$$

"Density" of carriers along *x* for any energy level

Landau levels

D'altra parte, l'energia del portatore di carica si può scrivere

$$E = E_n + \frac{\hbar^2 k_z^2}{2m}\,, \qquad (14)$$

dove rispetto alla Eq. (14) si è esplicitata la parte cinetica. Dalla Eq. (14) si ricava

$$dk_z = \frac{\sqrt{2m}}{2\hbar}\frac{1}{\sqrt{E-E_n}}dE \qquad (15)$$

da cui

$$g(E) \propto \frac{1}{\sqrt{E-E_n}}\,, \qquad (16)$$

densità degli stati tipica per un gase 1-DEG. In corrispondenza delle energie E_n la $g(E)$ tende a divergere (livelli di Landau).

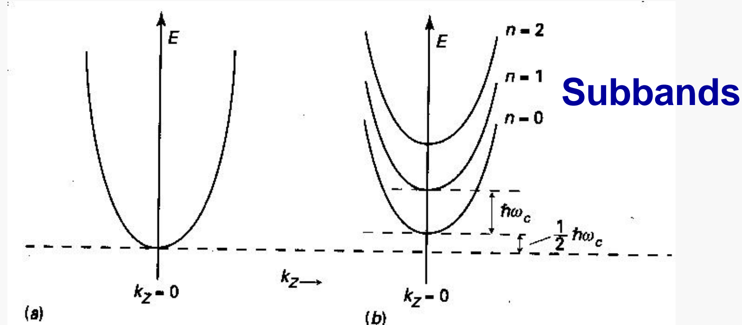

Subbands

Figura 9.3
Schema di bande di energia in funzione di k_z in assenza (a) ed in presenza (b) di un campo magnetico $\overline{B}$ applicato in direzione z (vedi eq. 9.52).

1D-like density of states

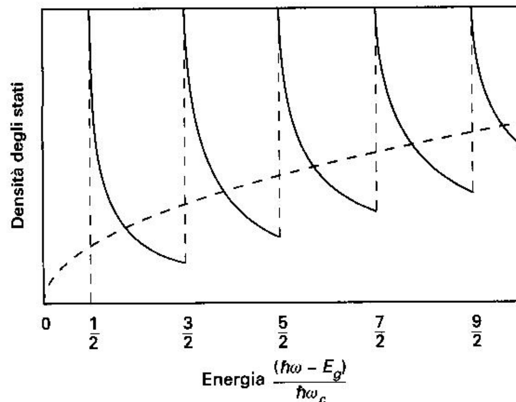

Figura 9.5
Densità di stati vicino al minimo di una banda in presenza di un campo magnetico costante: il caso $B = 0$ è indicato con linea tratteggiata (vedi eq. 8.25) e il caso $B \neq 0$ con linea continua (vedi eq. 9.58).

(Surface) carrier density, corresponding to each Landau level is *eB/h*

Density of states diverges at the energy level "bottom"

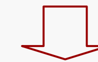

For a *given number of carriers* (electrons), **a B value exists** (in principle) so that ***all* carriers** are in the ground level

The small thickness of the conductor combined with the presence of the magnetic field leads to a 1D-like behavior

QHE and von Klitzing quantum of resistance I

0.4 Quanto di resistenza di Von Klitzing

Considerando la forza di Lorentz come forza elettromotrice, nell'effetto Hall classico si ha che la differenza di potenziale V_H (in direzione y, cioè trasversa rispetto al moto delle cariche e al campo magnetico) è $V_H = LBv$ e la corrente di portatori di carica è $I = n_s veL$, con n_s densità superficiale di carica già introdotta. Dalla legge di Ohm si deduce una resistenza Hall R_H:

$$R_H = \frac{V_H}{I} = \frac{B}{n_s e} . \qquad (17)$$

Nel QHE, l'azione combinata del campo magnetico e del confinamento spaziale porta alla presenza dei livelli di Landau e alla loro degenerazione. Quando un livello di Landau (supponiamo il livello m) è completamente occupato e il successivo è completamente vuoto, cioè m livelli di Landau sono pieni, ognuno con la degenerazione vista in precedenza, allora, secondo la Eq. (13), si avrà un numero di elettroni per unità di superficie pari a:

$$n = m\frac{eB}{h} , \qquad (18)$$

da cui deriva che la resistenza Hall si esprime come sottomultiplo del valore h/e^2, dipendente solo da costanti fondamentali:

$$R_H = \frac{1}{m}\frac{h}{e^2} . \qquad (19)$$

Fine structure constant

Questo risultato ha diverse conseguenze. In primo luogo stabilisce un valore quantizzato della resistenza (il cui valore è 25812.806 ohm). Occorre notare che nell'effetto Hall quantistico la quantizzazione della resistenza è conseguenza del confinamento spaziale, ma la sua osservazione è resa possibile dalla presenza del campo magnetico (e conseguente quantizzazione del moto dei portatori di carica). In condizioni ordinarie l'effetto di quantizzazione non è facilmente osservabile (e, in generale, si ricordi che la resistenza misurata può essere interpretata come un parallelo di tante resistenze). Inoltre esistono delle conseguenze notevoli dal punto di vista metrologico, legate alla precisione con cui si può eseguire la misura delle costanti fondamentali h e e^2. Dal punto di vista tecnologico, la conseguenza principale è comunque che la differenza di potenziale misurata non è lineare con la corrente, ma segue un tipico andamento a gradini. Per ragioni di tipo sperimentale, i sistemi in cui tradizionalmente si osserva QHE sono delle eterostrutture, ad esempio tipo GaAs/GaAsAl, in cui il confinamento spaziale è ottenuto in strati sottili (pozzi quantici).

Per completezza, occorre ricordare che accanto al QHE *intero*, scoperto da Von Klitzing (premio Nobel 1985), esiste un QHE *frazionario*, legato all'occupazione frazionaria dei livelli di Landau (Tsui and Stormer, premio Nobel 1998).

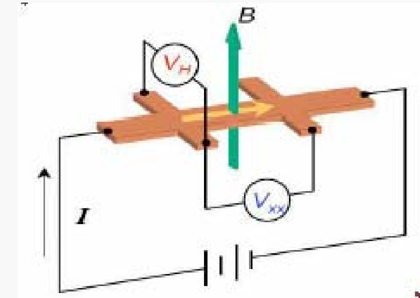

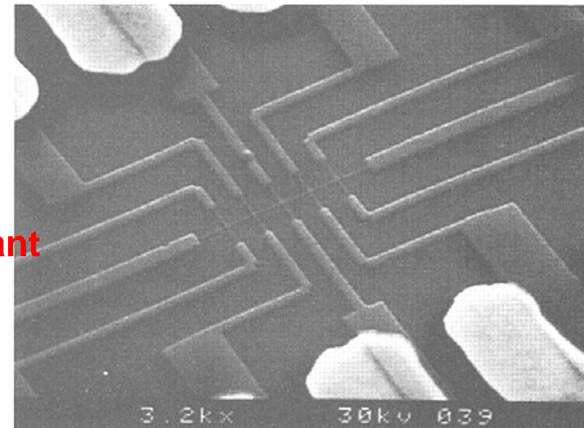

Fig. 0.3. Scanning electron micrograph of a long wire 75 nm wide patterned from a GaAs–AlGaAs heterojunction. Four-terminal Hall measurements are made using voltage probes placed along the wire ~ 2 μm. apart. Reproduced with permission from M. L. Roukes, A. Scherer, S. J. Allen, H. G. Craighead, R. M. Ruthen, E. D. Beebe and J. P. Harbison (1987), *Phys. Rev. Lett.* **59**, 3011.

Measurements carried out at very low temperature in order to decrease (phonon) scattering

QHE and von Klitzing quantum of resistance II

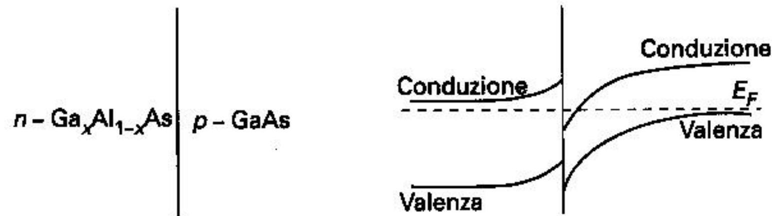

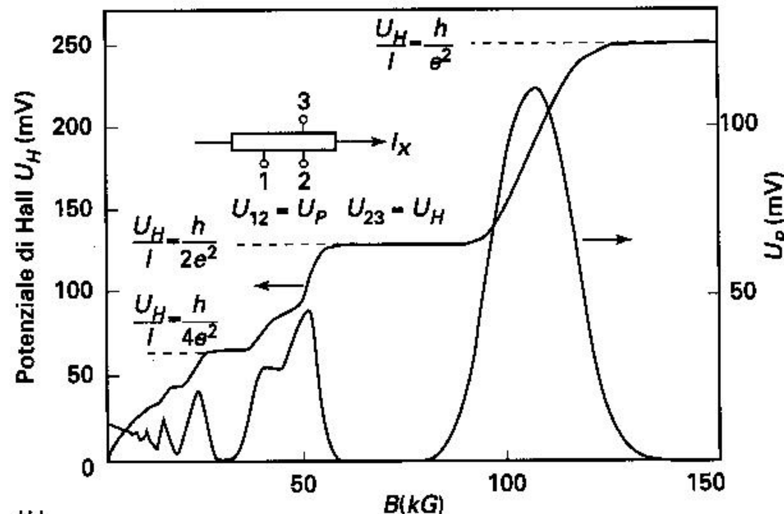

Figura 11.11
(*a*) Indicazione schematica della giunzione con campo elettrico, che produce stati con mobilità alla superficie della giunzione. (*b*) Misure di effetto Hall quantizzato, con i caratteristici gradini dove il potenziale di Hall è costante, e il potenziale nella direzione della corrente è nullo. (Da K. von Klitzing, Europhysics News **13**, 2 (Aprile 1982)).

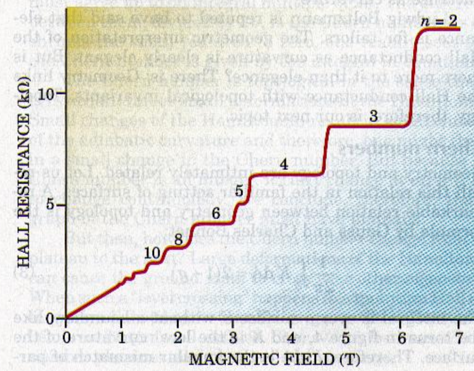

Figure 2. The integer quantum Hall effect. Plotting the Hall resistance (essentially the reciprocal of the Hall conductance) of a low-temperature two-dimensional electron gas against the strength of the imposed magnetic field normal to the gas plane, one finds a stairlike quantized sequence of Hall conductances very precisely equal to ne^2/h, where n is the integer that characterizes each plateau. The natural unit of resistance defined by this effect is about 26 kΩ. (Adapted from M. Paalanen, D. Tsui, A. Gossard, *Phys. Rev. B.* **25**, 5566 [1982].)

http://www.physicstoday.org August 2003 Physics Today 39

Resistance is quantized in units of R_{vk}= h/e^2 ~ 25.8 Kohm

The quantum depends on the fine structure costant, i.e., on fundamental quantities (*e, h*)

A few words on fractional-QHE

1982 (Tsui, Stoermer, et al.): discovery of Fractional-QHE

$$R_H = \frac{p}{q}\frac{h}{e^2}$$

$$\nu = \frac{p}{2mp \pm 1}$$

Filling factor

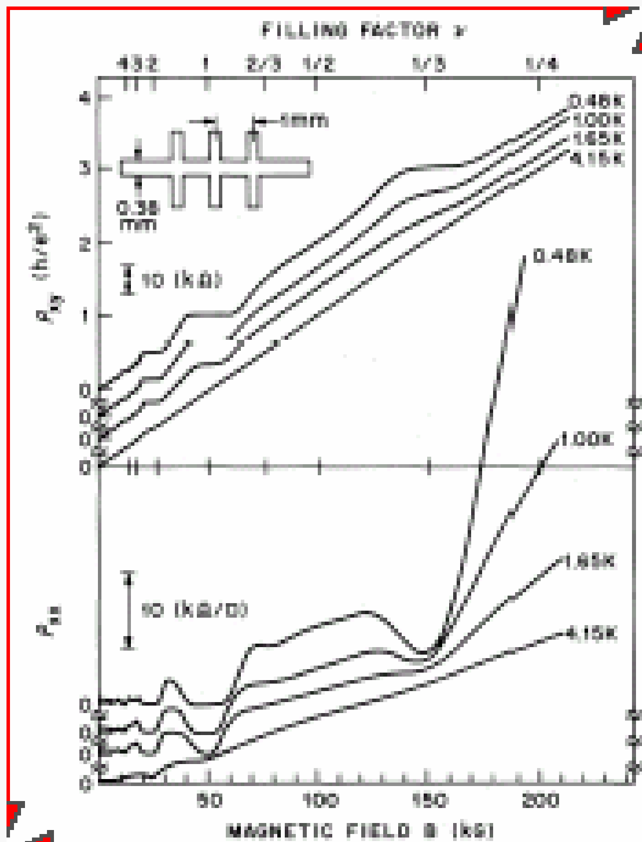

Tsui et al., PRL 48, 1559 (1982)

Interpretation (Laughlin): many-body problem

The Hamiltonian should include terms accounting for interaction inter-electron and electron-ion (lattice)

A collective wavefunction (product of single electron wavefunction) should be used and the corresponding Landau levels identified

Degeneracy of the levels turns out to depend on the specific system considered

B. Towards 1DEG

We have seen that 2DEG structures *with* magnetic field **B** do exhibit quantized transport behavior (von Klitzing quantum of resistance)

Role of **B**: to mix up directions so that 2DEG behaves similarly to 1DEG

If **B** = 0 no quantum effect is observed (the charge carriers can always find a "non confined" direction for their motion!)

1DEG structures (**quantum wires**) are thus expected to show a signature of quantum confinement effects *without* **B**

From the technological point of view, a 1DEG is quite complicated to achieve in "conventional" electronics (inorganics), but it can be done

The simplest way, at least ideally, is based on the exploitation of either **linear conductive molecules** (organics) or **mesoscopic structures** (nanowires/nanotubes): we will see more!

Examples of realization of 1-D nanostructures (conventional) I

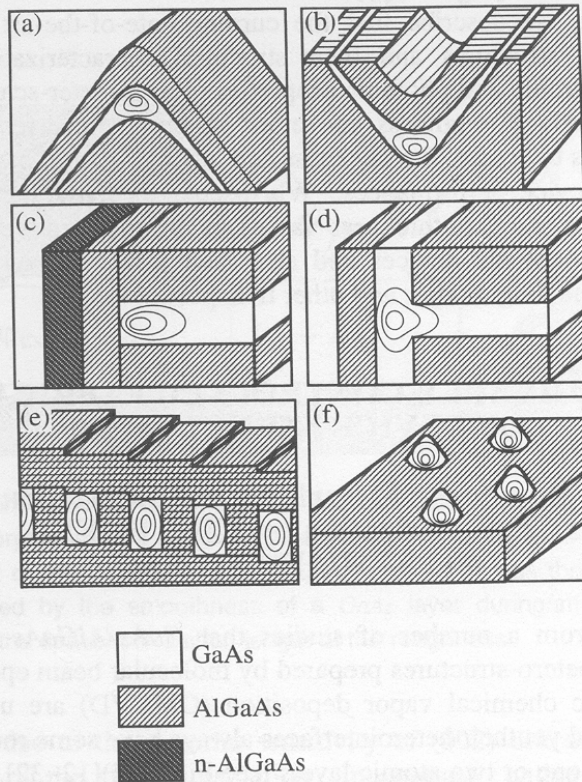

FIGURE 3. Examples of epitaxially grown QWRs and QBs. A ridge QWR (a), a groove QWR (b), a (field-induced) edge QWR (c), a (T-shaped) edge QWR (d), a tilted superlattice (TSL) (e), and a self-assembled QB structure (f). See section VI.B for their details and references.

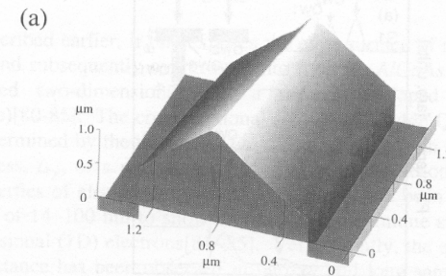

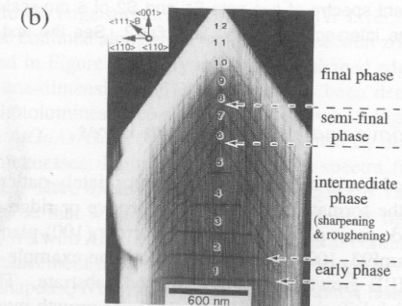

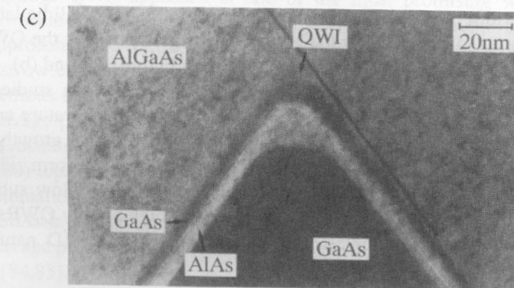

FIGURE 20. (a) An AFM image of an MBE grown *GaAs* ridge. (b)An SEM cross-sectional image of a *GaAs* ridge with thin *AlAs* marker layers. (c)A TEM image of a ridge quantum wire structure after Koshiba *et al.*[97]. (See color plate.)

Film growth with specific arrangements
(e.g., onto specifically "cut" susbtrates)

Examples of realization of 1-D nanostructures (lithography) II

Figure 16: Schematic cross sectional views of three different ways to define narrow 2-DEG channels in an AlGaAs/GaAs heterostructure. The positively ionized donors and the negatively charged 2-DEG channel as well as the negative Schottky gate electrode (b) are indicated.
(a) Lithographically structured wire on a modulation doped (AlGaAs n-doped) AlGaAs/GaAs heterostructure.
(b) 2-DEG channel formed in the 2-DEG at an AlGaAs/GaAs heterostructure by the action of two evaporated metal gates. If biased negatively they repel the electrons in the 2-DEG below.
(c) A similar effect on the electron concentration in the 2-DEG is obtained by spatially varying ionized donor concentration (positive charges) in the upper AlGaAs layer.

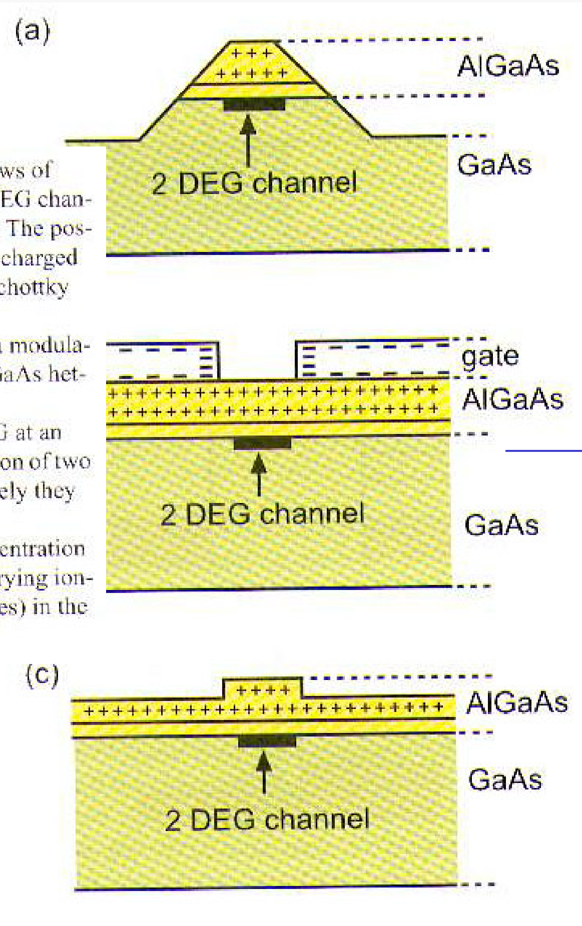

Split-gate MODFET

(MOdulation Doping)

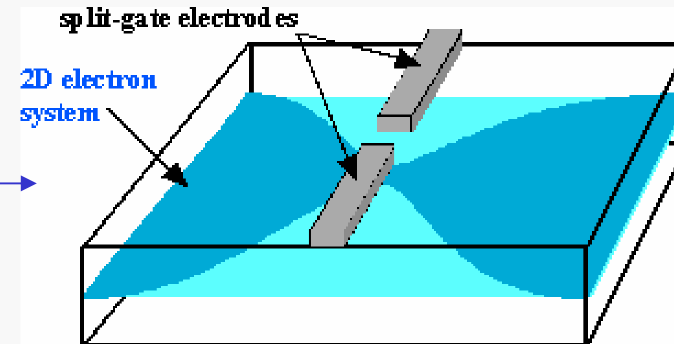

An additional pair of electrodes with a nanosized gap leads to a 1-D like conducting channel

Da R. Waser Ed., Nanoelectronics and information technology (Wiley-VCH, 2003)

Lithography (typically EBL) used to define laterally the structure

A closer look at the de Broglie wavelength

Degenerate and non-degenerate conductors

At equilibrium the available states in a conductor are filled up according to the Fermi function

$$f_0(E) = \frac{1}{1+\exp[(E-E_f)/k_BT]} \quad (1.2.7)$$

where E_f is the Fermi energy. Away from equilibrium the system has no common Fermi energy, but often we can talk in terms of a local quasi-Fermi level which can vary spatially and which can be different for different groups of states (such as electrons and holes) even at the same spatial location. We will generally use F_n to denote quasi-Fermi levels and reserve E_f for the equilibrium Fermi energy.

There are two limits in which the Fermi function inside the band $(E > E_s)$ can be simplified somewhat making it easier to perform numerical calculations (see Fig. 1.2.2). One is the high temperature or the non-degenerate limit ($\exp[E_s - E_f]/k_BT >> 1$) where

$$f_0(E) \approx \exp[-(E-E_f)/k_BT] \quad (1.2.8)$$

(a) Non-degenerate limit

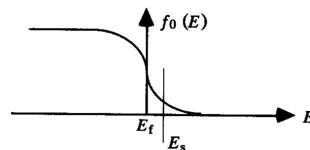

(b) Degenerate limit

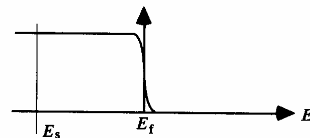

Fig. 1.2.2. The Fermi function inside the band ($E > E_s$) can be approximated by (*a*) Eq.(1.2.8) in the non-degenerate limit and (*b*) by Eq.(1.2.9) in the degenerate limit.

The other is the low temperature or the degenerate limit ($\exp[E_s - E_f]/k_BT << 1$) where

$$f_0(E) \approx \vartheta(E_f - E) \quad (1.2.9)$$

In this book we will mainly be discussing degenerate conductors.

To relate the equilibrium electron density n_s (per unit area) to the Fermi energy we make use of the relation

$$n_s = \int N(E) f_0(E) \mathrm{d}E$$

For degenerate conductors it is easy to perform the integral to obtain

$$n_s = N_s(E_f - E_s) \quad \text{where} \quad N_s \equiv m/\pi\hbar^2 \quad (1.2.10)$$

where we have made use of Eqs.(1.2.6) and (1.2.9).

At low temperatures the conductance is determined entirely by electrons with energy close to the Fermi energy. The wavenumber of such electrons is referred to as the Fermi wavenumber (k_f):

$$E_f - E_s = \frac{\hbar^2 k_f^2}{2m} \Rightarrow \hbar k_f = \sqrt{2m(E_f - E_s)} \quad (1.2.11)$$

Using Eq.(1.2.10) we can express the Fermi wavenumber in terms of the electron density:

$$k_f = \sqrt{2\pi n_s} \quad (1.2.12)$$

The corresponding velocity is the Fermi velocity $v_f = \hbar k_f / m$.

In the "degenerate case" (low temperature) Fermi velocity depends on the square root of the electron density

Criteria for 1DEG situations

1.3 Characteristic lengths

A conductor usually shows ohmic behavior if its dimensions are much larger than certain characteristic lengths, namely, (1) the de Broglie wavelength, (2) the mean free path, and (3) the phase-relaxation length. We will discuss these one by one. In addition to these characteristic lengths, the screening length can also play a significant role especially in low-dimensional conductors as we will see in Section 2.3 (see Fig. 2.3.3).

Wavelength (λ)

We have seen (Eq.(1.2.12)) that the Fermi wavenumber k_f goes up as the square root of the electron density. The corresponding wavelength goes down as the square root of the electron density:

$$\lambda_f = 2\pi/k_f = \sqrt{2\pi/n_s} \tag{1.3.1}$$

De Broglie wavelength at the Fermi velocity

For an electron density of $5 \times 10^{11}/\text{cm}^2$, the Fermi wavelength is about 35 nm. At low temperatures the current is carried mainly by electrons having an energy close to the Fermi energy so that the Fermi wavelength is the relevant length. Other electrons with less kinetic energy have longer wavelengths but they do not contribute to the conductance.

Mean free path (L_m)

An electron in a perfect crystal moves as if it were in vacuum but with a different mass. Any deviation from perfect crystallinity such as impurities, lattice vibrations (phonons) or other electrons leads to 'collisions' that scatter the electron from one state to another thereby changing its momentum. The momentum relaxation time τ_m is related to the collision time τ_c by a relation of the form

$$\frac{1}{\tau_m} \rightarrow \frac{1}{\tau_c}\alpha_m$$

where the factor α_m (lying between 0 and 1) denotes the 'effectiveness' of an individual collision in destroying momentum. For example if the collisions are such that the electrons are scattered only by a small angle then very little momentum is lost in an individual collision. The factor α_m is then very small so that the momentum relaxation time is much longer than the collision time. For a more detailed discussion of scattering times in semiconductors see, for example, Chapter 4 of S. Datta (1989), *Quantum Phenomena*, Modular Series on Solid-state Devices, vol. VIII, eds. R. F. Pierret and G. W. Neudeck, (New York, Addison–Wesley).

The mean free path, L_m, is the distance that an electron travels before its initial momentum is destroyed; that is,

$$L_m = v_f\,\tau_m \tag{1.3.2}$$

where τ_m is the momentum relaxation time and v_f is the Fermi velocity. The Fermi velocity is given by

$$v_f = \frac{\hbar k_f}{m} = \frac{\hbar}{m}\sqrt{2\pi n_s} \rightarrow 3\times 10^7\,\text{cm/s} \quad \text{if} \quad n_s = 5\times 10^{11}/\text{cm}^2$$

Assuming a momentum relaxation time of 100 ps we obtain a mean free path of $L_m = 30\ \mu\text{m}$.

Phase-relaxation length (L_φ)

Let us first discuss what is meant by the phase-relaxation time (τ_φ). We will then relate it to the phase-relaxation length. In analogy with the momentum relaxation time we could write

$$\frac{1}{\tau_\varphi} \rightarrow \frac{1}{\tau_c}\alpha_\varphi$$

where the factor α_φ denotes the effectiveness of an individual collision in destroying phase. The destruction of phase is, however, a little more subtle than the destruction of momentum. A more careful discussion is required to define what the effectiveness factor α_φ is for different types of scattering processes.

1DEG conditions can be achieved only "on a short path"

A rough picture of transport in 1DEG

In the bulk, classically we have:
$\boldsymbol{J} = n\ e\ \boldsymbol{v}$

1. At T=0 only the portion of electrons $eV/\ E_F$ is involved in the transport process
2. Fermi velocity must be considered: $v_F = \sqrt{(2E_F/m)}$;
3. n $\propto \int g(E)dE$; in the 1-D case $\propto \sqrt{E_F}$

$I = eV/E_F\ e\ \sqrt{(2E_F/m)}\ \sqrt{(2m\ E_F)}/h =$
$= 2\ e^2\ V/h$

Conductivity in an ideal 1DEG structure:
$\boldsymbol{G_{1D} = i/V = 2\ e^2/h}$

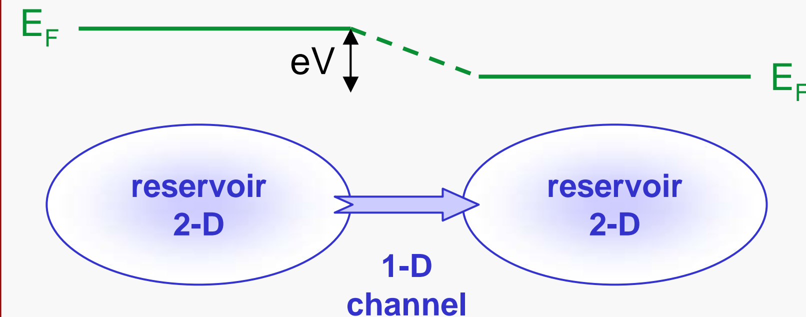

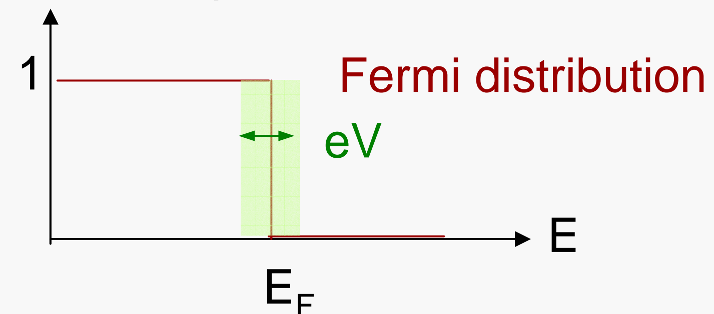

1DEG DOS peculiarities lead to a quantized conductivity

See van Wees et al.
PRL 60 848 (1988)

Landauer levels (intrawire tunneling)

"tunneling" through a quantum wire

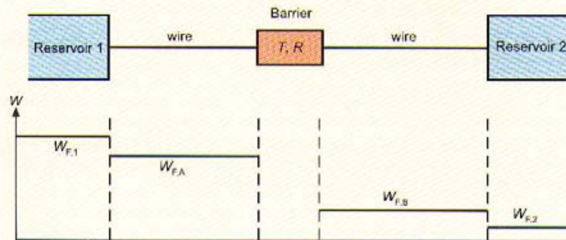

Figure 19: One-channel model for the derivation of ballistic quantum transport through a barrier between two reservoirs. The barrier is described by its transmittance T and its reflectance R. μ_1, μ_2, μ_A and μ_B are the chemical potentials in the different regions.

A general description of non-diffusive quantum-mechanical transport in nano- and mesoscopic structures has been developed by Landauer [9] and Büttiker [10]. In the idealized model two reservoirs 1 and 2 characterized by their chemical potentials $W_{F,1}$ and $W_{F,2}$ are connected through two ideal 1-D wires of length L. In these wires the electronic states are plane waves $\psi(x) = \exp(ikx)/\sqrt{L}$, which can have positive and negative k-vectors and two spin orientations. With the quantum-mechanical expression for the current density in one dimension

$$j = \frac{e\hbar}{2im}\left(\psi^*\nabla\psi - \psi\nabla\psi^*\right) \tag{55}$$

(quantum) current density

the corresponding current for one k-vector and one spin orientation is obtained as

$$I = \frac{e\hbar k}{mL} \tag{56}$$

Between the two wires an energetic barrier for the electrons is assumed, which is characterized by its quantum-mechanical reflection coefficient R and its transmission coefficient T, with $T + R = 1$ (Figure 19).

Due to the difference $W_{F,1}-W_{F,2}$ of the chemical potentials a current through the wires is induced. It results from electrons with energies $W_{F,1} \geq W \geq W_{F,2}$ and k-vectors in positive forward direction, which occupy the electronic states in the left wire. Part of the current is reflected at the barrier and the other part is transmitted. The reflected current is absorbed in reservoir 1 while the transmitted part is absorbed in reservoir 2. Only within these reservoirs does energy dissipation occur. The total current in the positive k-direction in the left wire is thus obtained by adding up all occupied states and using (56) as

$$I_{\rightarrow} = \frac{e\hbar k}{mL} L D^{(1)}(W)\left(W_{F,1} - W_{F,2}\right) \tag{57}$$

$D^{(1)}(W)$ is the 1-D density of states (per wire length L) according to (51). With $W = \hbar^2k^2/2m$ this yields

$$I_{\rightarrow} = \frac{e}{\pi\hbar}(W_{F,1} - W_{F,2}) \tag{58}$$

and for the transmitted net current in the right wire

$$I = \frac{e}{\pi\hbar}T\left(W_{F,1} - W_{F,2}\right) \tag{59}$$

The reflected current I_R in the left wire is accordingly

$$I_R = \frac{e}{\pi\hbar}R\left(W_{F,1} - W_{F,2}\right) \tag{60}$$

For the determination of the chemical potentials the total number of states in the wires, with positive and negative k-values, has to be taken into account, i.e. $2D^{(1)}(W)(W_{F,1}-W_{F,2})$. In the right wire the current, which is induced by $(W_{F,1}-W_{F,2})$, corresponds to a complete occupation of states between $W_{F,B}$ and $W_{F,2}$ (Figure 19), such that

$$TD^{(1)}(W)\left(W_{F,1} - W_{F,2}\right) = 2D^{(1)}(W)\left(W_{F,1} - W_{F,2}\right) \tag{61}$$

Within the left wire both the currents $I_{\rightarrow}$ and I_R have to be considered and the resulting occupation of states is assumed to correspond to the occupation of states between $W_{F,A}$ and $W_{F,2}$, such that

$$(1+R)D^{(1)}(W)\left(W_{F,1} - W_{F,2}\right) = 2D^{(1)}(W)\left(W_{F,A} - W_{F,2}\right) \tag{62}$$

With R+T = 1 the difference between (61) and (62) yields

$$W_{F,A} - W_{F,B} = R\left(W_{F,1} - W_{F,2}\right) \tag{63}$$

With V as the voltage between both wires and $eV = W_{F,A} - W_{F,B}$ one obtains from (59) and (63) for the current through the wires

$$I = \frac{e^2}{\pi\hbar}\frac{T}{R}V = \frac{2e^2}{h}\frac{T}{R}V \tag{64}$$

This is the analogue to Ohm's law for quantum transport through a nanoscopic system. The conductance of the system thus follows as

$$G = \frac{2e^2}{h}\frac{T}{R} \tag{65}$$

This so-called Landauer formula again contains the conductivity quantum e^2/h of 1-D quantum transport. The Landauer formalism for quantum transport can be generalized to a network where several wires connect a barrier with reservoirs.

Da R. Waser Ed., Nanoelectronics and information technology (Wiley-VCH, 2003)

Ballistic transport

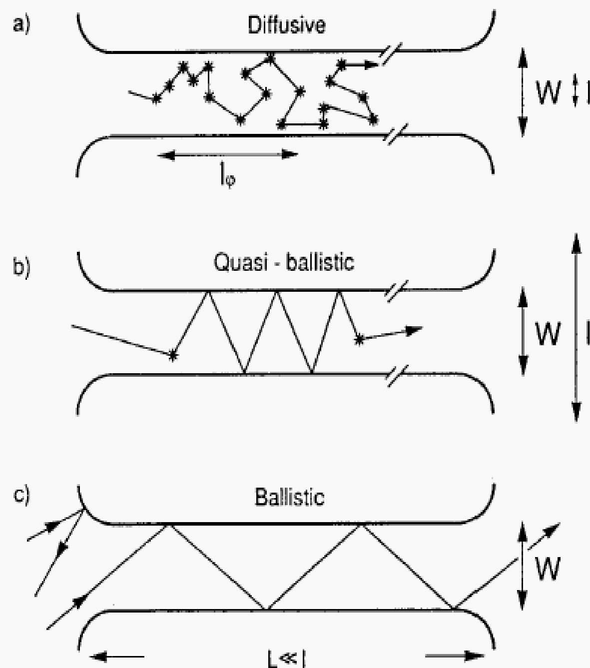

Figure 10.4: Electron trajectories characteristic of the diffusive ($\ell < W, L$), quasi-ballistic ($W < \ell < L$), and ballistic ($W, L < \ell$) transport regimes, for the case of specular boundary scattering. Boundary scattering and internal impurity scattering (asterisks) are of equal importance in the quasi-ballistic regime. A nonzero resistance in the ballistic regime results from backscattering at the connection between the narrow channel and the wide 2DEG regions. Taken from H. Van Houten et al. in "Physics and Technology of Submicron Structures" (H. Heinrich, G. Bauer and F. Kuchar, eds.) Springer, Berlin, 1988.

In the ballistic transport regime, electrons are assumed to move within the structure without scattering (but that at the interface with the ohmic contacts, i.e., the higher-dimensional "outer world")

Behavior analogous to an optical fiber in the total reflection mode

If a quantum wire is considered, comparison between the de Broglie wavelength and the *transverse* size suggests to consider *single mode fibers*

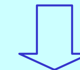

Transverse modes

Transverse modes I

1.6 Transverse modes (or magneto-electric subbands)

this section we will discuss the concept of transverse modes or sub-
ıds which will appear repeatedly in this book. These are analogous to
transverse modes (TE_{10}, TM_{11} etc.) of electromagnetic waveguides. In
row conductors, the different transverse modes are well separated in
ergy and such conductors are often called *electron waveguides*.

We consider a rectangular conductor that is uniform in the x-direction and has some transverse confining potential $U(y)$ (see Fig. 1.6.1). The motion of electrons in such a conductor is described by the effective mass equation (see Eq.(1.2.2))

$$\left[E_s + \frac{(i\hbar\nabla + e\mathbf{A})^2}{2m} + U(y)\right]\Psi(x,y) = E\Psi(x,y)$$

We assume a constant magnetic field B in the z-direction perpendicular to the plane of the conductor. This can be represented by a vector potential of the form

$$\mathbf{A} = -\hat{x}By \quad \Rightarrow \quad A_x = -By \quad \text{and} \quad A_y = 0$$

so that Eq.(1.2.2) can be rewritten as

$$\left[E_s + \frac{(p_x + eBy)^2}{2m} + \frac{p_y^2}{2m} + U(y)\right]\Psi(x,y) = E\Psi(x,y) \qquad (1.6.1)$$

where $\quad p_x = -i\hbar\frac{\partial}{\partial x} \quad$ and $\quad p_y = -i\hbar\frac{\partial}{\partial y}$

The solutions to Eq.(1.6.1) can be expressed in the form of plane waves (L: length of conductor over which the wavefunctions are normalized)

$$\Psi(x,y) = \frac{1}{\sqrt{L}}\exp[ikx]\chi(y) \qquad (1.6.2)$$

where the transverse function $\chi(y)$ satisfies the equation

$$\left[E_s + \frac{(\hbar k + eBy)^2}{2m} + \frac{p_y^2}{2m} + U(y)\right]\chi(y) = E\chi(y) \qquad (1.6.3)$$

Note that the choice of vector potential is not unique for the given magnetic field. For example we could choose $A_x = 0$ and $A_y = -Bx$. The solutions would then look very different though the physics of course must remain the same. It is only with our choice of gauge, that the solutions have the form of plane waves in the x-direction. We will use this gauge in all our discussions.

We are interested in the nature of the transverse eigenfunctions and the eigenenergies for different combinations of the confining potential U and the magnetic field B. In general for arbitrary confinement potentials $U(y)$

ere are no analytical solutions. However, for a parabolic potential
hich is often a good description of the actual potential in many elec-
on waveguides)

$$U(y) = \frac{1}{2}m\omega_0^2 y^2$$

Model confining potential

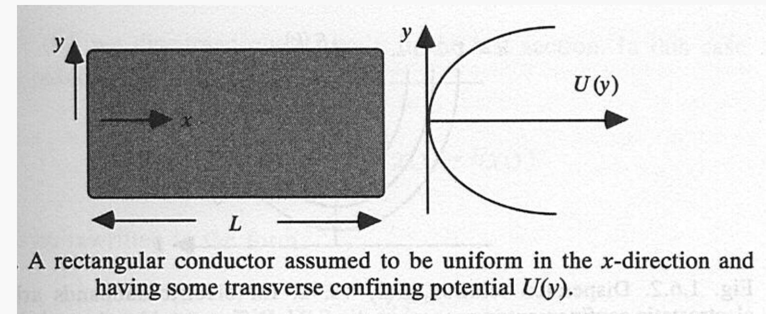

A rectangular conductor assumed to be uniform in the x-direction and having some transverse confining potential $U(y)$.

Electrons are confined within the structure by a suitable potential

The "transverse eigenfunction" (depending on the potential) must obey the boundary conditions

Transverse modes II

Confined electrons (U ≠ 0) in zero magnetic field (B = 0)

onsider first the case of zero magnetic field, so that Eq.(1.6.3) reduces

$$\left[E_s + \frac{\hbar^2 k^2}{2m} + \frac{p_y^2}{2m} + \frac{1}{2} m\omega_0^2 y^2\right]\chi(y) = E\chi(y) \qquad (1.6.4)$$

he eigenfunctions of Eq.(1.6.4) are well-known (see any quantum echanics text such as L. I. Schiff (1968), *Quantum Mechanics*, Third dition, (New York, McGraw–Hill) Section 13). The eigenenergies and genfunctions are given by

$$\chi_{n,k}(y) = u_n(q) \quad \text{where} \quad q = \sqrt{m\omega_0/\hbar}\, y \qquad (1.6.5a)$$

$$E(n,k) = E_s + \frac{\hbar^2 k^2}{2m} + \left(n + \tfrac{1}{2}\right)\hbar\omega_0, \quad n = 0,1,2,\ldots \qquad (1.6.5b)$$

Subbands

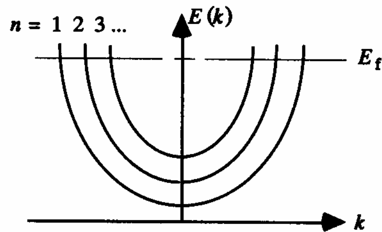

Fig. 1.6.2. Dispersion relation, $E(k)$ vs. k. for electric subbands arising from electrostatic confinement in zero magnetic field. Different subbands are indexed by n.

where $$u_n(q) = \exp\left[-q^2/2\right] H_n(q)$$

$H_n(q)$ being the nth Hermite polynomial. The first three of these polynomials are

$$H_0(q) = \frac{1}{\pi^{1/4}}, \quad H_1(q) = \frac{\sqrt{2}q}{\pi^{1/4}} \quad \text{and} \quad H_2(q) = \frac{2q^2 - 1}{\sqrt{2}\pi^{1/4}}$$

The velocity is obtained from the slope of the dispersion curve:

$$v(n,k) = \frac{1}{\hbar}\frac{\partial E(n,k)}{\partial k} = \frac{\hbar k}{m} \qquad (1.6.5c)$$

Group velocity

The dispersion relation is sketched in Fig. 1.6.2. States with different index n are said to belong to different subbands just like the subbands that arise from the confinement in the z-direction (see Section 1.2). The spacing between two subbands is equal to $\hbar\omega_0$. The tighter the confinement, the larger ω_0 is, and the further apart the subbands are. Usually the confinement in the z-direction is very tight (~ 5–10 nm) so that the corresponding subband spacing is large (~ 100 meV) and only one or two subbands are customarily occupied. Indeed, in all our discussions we will assume that only one z-subband is occupied. But the y-confinement is relatively weak and the corresponding subband spacing is often quite small so that a number of these are occupied under normal operating conditions. The subbands are often referred to as *transverse modes* in analogy with the modes of an electromagnetic waveguide.

After S.Datta, Electronic Transport in Mesoscopic Systems, Cmbridge (1997)

Quantization (subbands) arises when solving the Schroedinger equation in the confining potential (transverse modes)

Transverse modes III

Calculating the current

To calculate the current we note that the states in the narrow conductor belong to different transverse modes or subbands as discussed in Section 1.6. Each mode has a dispersion relation $E(N,k)$ as sketched in Fig. 2.1.1b with a cut-off energy

$$\varepsilon_N = E(N, k = 0)$$

below which it cannot propagate. The number of transverse modes at an energy E is obtained by counting the number of modes having cut-off energies smaller than E:

$$M(E) = \sum_N \vartheta(E - \varepsilon_N) \tag{2.1.1}$$

We can evaluate the current carried by each transverse mode (numbered by 'N' in Fig. 2.1.1b) separately and add them up.

Consider a single transverse mode whose $+k$ states are occupied according to some function $f^+(E)$. A uniform electron gas with n electrons per unit length moving with a velocity v carries a current equal to env. Since the electron density associated with a single k-state in a conductor of length L is $(1/L)$ we can write the current I^+ carried by the $+k$ states as

$$I^+ = \frac{e}{L}\sum_k v f^+(E) = \frac{e}{L}\sum_k \frac{1}{\hbar}\frac{\partial E}{\partial k} f^+(E)$$

Assuming periodic boundary conditions (see Fig. 1.2.1 and related discussion) and converting the sum over k into an integral according to the usual prescription

$$\sum_k \rightarrow 2 \text{ (for spin)} \times \frac{L}{2\pi}\int \mathrm{d}k$$

we obtain

$$I^+ = \frac{2e}{h}\int_\varepsilon^\infty f^+(E)\,\mathrm{d}E$$

where ε is the cut-off energy of the waveguide mode. We could extend this result to multi-moded waveguides and write the current, I^+, carried by the $+k$ states in a conductor as

$$I^+ = \frac{2e}{h}\int_{-\infty}^{+\infty} f^+(E) M(E)\,\mathrm{d}E \tag{2.1.2}$$

where the function $M(E)$ (defined in Eq.(2.1.1)) tells us the number of modes that are above cut-off at energy E. Note that this is a general result independent of the actual dispersion relation $E(k)$ of the waveguide: the current carried per mode per unit energy by an occupied state is equal to $2|e|/h$ (which is about 80 nA/meV).

Contact resistance

Assuming that the number of modes M is constant over the energy range $\mu_1 > E > \mu_2$, we can write

$$I = \frac{2e^2}{h} M \frac{(\mu_1 - \mu_2)}{e} \Rightarrow G_C = \frac{2e^2}{h} M \tag{2.1.3}$$

so that the contact resistance (which is the resistance of a ballistic waveguide) is given by

$$G_C^{-1} = \frac{(\mu_1 - \mu_2)/e}{I} = \frac{h}{2e^2 M} \approx \frac{12.9\,\mathrm{k\Omega}}{M}$$

Note that the contact resistance goes down inversely with the number of modes. The contact resistance of a single-moded conductor is ~ 12.9 kΩ, which is certainly not negligible! This is the resistance one would measure if a single-moded ballistic conductor were sandwiched between two conductive contacts.

Usually we are concerned with wide conductors having thousands of modes so that the contact resistance is very small and tends to go unnoticed. To calculate the number of modes $M(E)$ we need to know the cut-off energies for the different modes ε_N. As we have seen in Section 1.6, the details depend on the confining potential $U(y)$ and the magnetic field. However, for wide conductors in zero magnetic field the precise nature of the confining potential is not important. We can estimate the number of modes simply by assuming periodic boundary conditions. The allowed values of k_y are then spaced by $2\pi/W$ (see Fig. 1.2.1), with each value of k_y corresponding to a distinct transverse mode. At an energy E_f $(= \hbar^2 k_f^2/2m)$, a mode can propagate only if $-k_f < k_y < k_f$. Hence the number of propagating modes can be written as

$$M = \mathrm{Int}\left[\frac{k_f W}{\pi}\right] = \mathrm{Int}\left[\frac{W}{\lambda_f/2}\right]$$

where $\mathrm{Int}(x)$ represents the integer that is just smaller than x. Assuming a Fermi wavelength of 30 nm, the number of modes in a 15 μm wide field-effect transistor is approximately 1000, so that the contact resistance is about 12.5 Ω.

The waveguide supports trasnverse modes below some (energy) cut-off, leading to Landauer levels

Da G. Timp, Nanotechnology (Springer-Verlag, 1999)

Electron waveguides I

Da R. Waser Ed., Nanoelectronics and information technology (Wiley-VCH, 2003)

SPLIT GATE

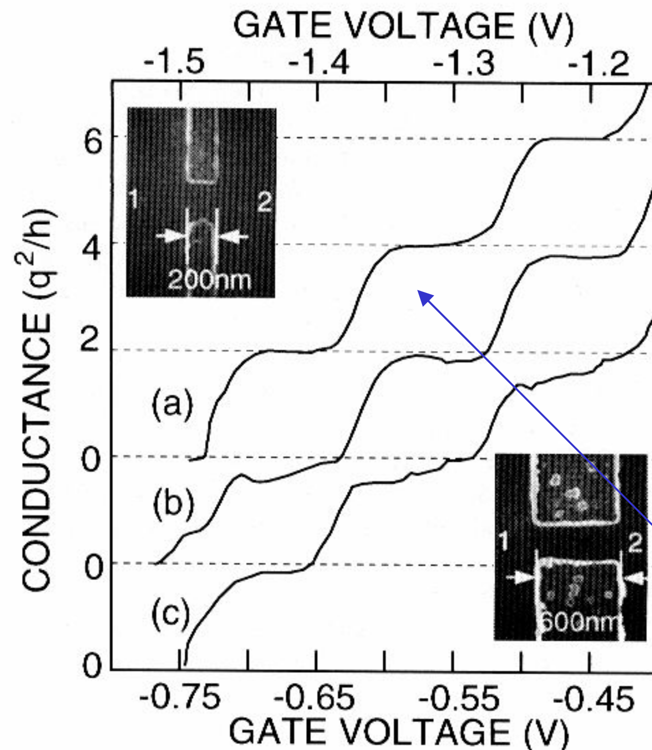

FIGURE 19. The two terminal conductance of an electron waveguide at T=280mK as a function of gate voltage (or the width of the constriction). The inset at the top of the figure shows a top view of 200 nm long split-gate electrodes with a 300 nm gap between them placed on a high mobility *GaAs/AlGaAs* heterostructure. The bottom inset shows a similar device on the same heterostructure with a 600 nm lithographic length. The quantization of the conductance ($\delta G = (1 \pm 0.01) 2q^2/h$) of the 200 nm long constriction shown in (a) deteriorates after cycling to room temperature, as shown in (b). We attribute the deterioration to a difference in the configuration of depletion charges corresponding variations in the width of the constriction. The poor quantization of the conductance of a 600 nm long constriction, shown in (c), is also supposed to develop from fluctuations in the width. (See color plate.)

POINT CONTACT (STM-like)

LANDAUER LEVELS

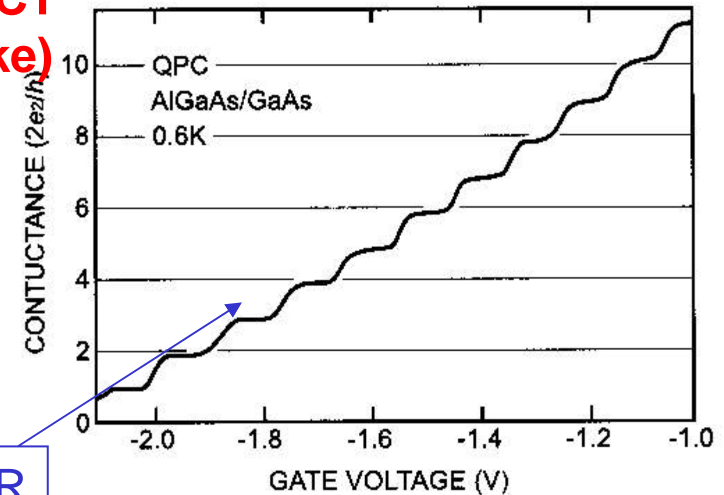

Figure 18: Quantized conductance of a quantum point contact (QPC) at 0.6K prepared at a AlGaAs/GaAs interface (2-DEG). The conductance was obtained from the measured resistance after subtraction of a constant series resistance of 400 Ω (After [8]).

Quantized resistance observed (at very low T)

Electron waveguides II

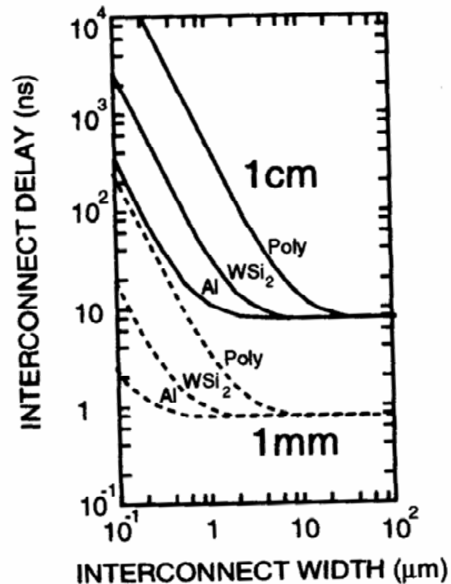

FIGURE 15. The interconnection delay for 1 cm and 1 mm long lines as a function of line width for three materials *Al*, WSi_2, and polysilicon assuming a channel resistance of $R_{ch} \approx 1k\Omega$. It is assumed that the spacing between lines is equal to the width, that the interconnection thickness is a third of the width, and that the dielectric thickness is about a fifth of the width. Constant field scaling is applied and we assume that $\rho_{Al} = 3\mu\Omega$cm, $\rho_{WSi_2} = 30\mu\Omega$cm, and $\rho_{Poly} = 500\mu\Omega$cm, for the respective resistivities. Adapted from Bakoglu[95].

If conductance is not affected by diffusive transport:
- resistance (within the wire) is negligible;
- speed is at a maximum;
- dissipation can be neglected;
- *single electron transport* can be achieved (no doubt a *single* charge entering the structure is transmitted!)

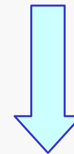

Quantum wire potentially suitable as unconventional interconnects (but cumbersome fabrication, need to operate at very low T!)

1DEG and active devices?

Can the 1DEG transport properties be exploited in a three-terminal (active) device?

Can a 1DEG-channel MOSFET (not just a split-gate) be realized?

[The idea is to control the few/single electron flow across the wire with an additional electric field or voltage]

We will see in “non conventional” implementations!
(possibly with less fabrication problems)

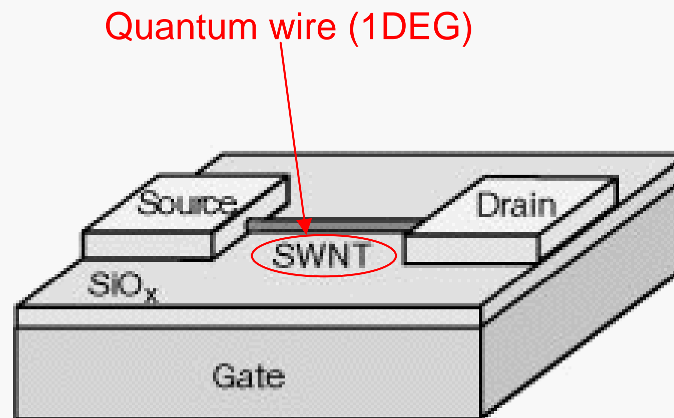

C. Towards 0DEG: a nanosized capacitor

Capacitance of a nanosized conducor (e.g., a metal) sphere

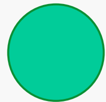

$Q = C\,V$
$V = Q/4\pi\varepsilon_0 r$
$C = 4\pi\varepsilon_0 r$
$E = CV^2/2$

Es.: if r~10 nm, C ~ 1 aF
At V = 1V Q ~ 10^{-18} Coulomb
That is N ~ 6 e !!!

The discrete nature of electric charge dominates the behavior of nanosized capacitors

In systems of very small conductors, the capacitances approach values sufficiently small that the charging energy given by (4.47) due to a single electron, $e^2/2C$, becomes comparable to the thermal energy, $k_B T_l$. The transfer of a single electron between conductors therefore results in a voltage change that is significant compared to the thermal voltage fluctuations and creates an energy barrier to the further transfer of electrons. This barrier remains until the charging energy is overcome by sufficient bias. How small must such a structure be? A simple example is the case of a conducting sphere above a grounded conducting plane. This example approximates a metal cluster imbedded in an insulator above a conducting substrate, which is a commonly realized structure that has been extensively studied experimentally. The exact solution may be found using the method of images, which gives the capacitance of the sphere as [33]

$$C = 4\pi\epsilon a\left(1 + \alpha + \frac{\alpha^2}{1-\alpha^2} + \cdots\right), \quad \alpha = \frac{a}{2l}, \tag{4.50}$$

where a is the radius of the sphere and l is the distance above the conducting substrate. As the radius of the sphere becomes small compared to l, the capacitance becomes independent of the distance of the cluster from the substrate. An alternate example is that of a flat circular disk located parallel to and a distance d above a ground plane. This example is more closely analogous to the semiconductor quantum dots fabricated by lateral confinement of a 2DEG as discussed in the previous sections. The solution is given in a problem in Jackson's textbook [34] (which we leave as an exercise for the reader!), with the capacitance given in the limit of $d \gg R$ as

$$C = 8\epsilon R \tag{4.51}$$

where R is the radius of the disk. Equating the charging energy with the thermal energy, we see that at room temperature, $C \sim 3 \times 10^{-18}$ F. The corresponding radius for a sphere from (4.50) is on the order of $a \sim 28$ nm (assuming a relative dielectric constant of 1), and somewhat larger for the disk. The facts that $\epsilon > \epsilon_o$ in real structures and that the charging energy should be several times larger than the thermal energy imply that sub-10-nm structures need to be fabricated in order to see clear single-electron charging effects at room temperature. Although it is still somewhat challenging with today's lithographic techniques to nanoengineer such structures, it is not difficult to grow insulating films with random metallic clusters on this order in which Coulomb blockade effects are readily observed, even at room temperature. Further, if we perform measurements at cryogenic temperatures, then the size scale becomes comparably larger, allowing single-electron effects to be observed in nanofabricated quantum dot structures.

Accurate capacitance evaluation for realistic cases

After Ferry and Goodnick,
Transport in nanostructures,
Cambridge (1997)

Tunneling rules the behavior of the system

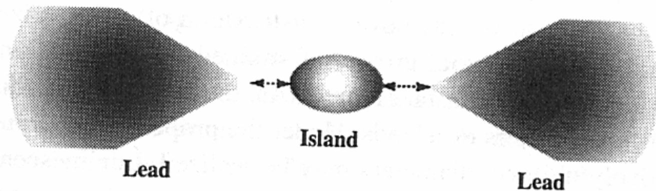

Tunneling inherently involved in "charging" the capacitor

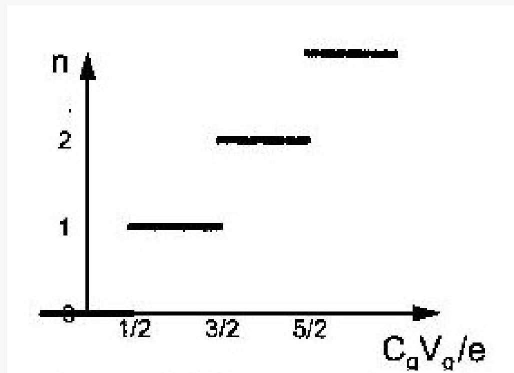

Figure 2: Electron number versus gate voltage characteristics of single-electron box. The number of electron in the quantum dot increases one by one as the gate voltage increases.

$$Q = CV \tag{4.46}$$

where C is the capacitance, Q is the charge on the conductor, and V the electrostatic potential relative to some chosen reference (e.g., ground). Since we are considering an ideal conductor, any charge added to the conductor rearranges itself such that the electric field inside vanishes, and the surface of the conductor becomes an equipotential surface. Therefore, the electrostatic potential associated with the conductor relative to its reference is uniquely defined. If we consider two conductors connected by a d.c. voltage source, a voltage $+Q$ builds up on one conductor and a charge $-Q$ on the other. The capacitance of the two conductor system is then defined as $C = Q/V_{12}$. The electrostatic energy stored in the two conductor system is the work done in building up the charge Q on the two conductors and is given by

$$E = \frac{Q^2}{2C}. \tag{4.47}$$

Electrostatic energy

For a system of N conductors, the charge on conductor i may be written

$$Q_i = \sum_{j=1}^{N} C_{ij} V_j, \tag{4.48}$$

where the diagonal values C_{ii} are the capacitance of conductor i if all other conductors are grounded. The diagonal elements are commonly referred to as the *coefficients of capacitance*; the off-diagonal elements are called the *coefficients of induction*. The total electrostatic energy stored in a multiconductor system is given by the generalization of Eq. (4.47) as

$$E = \frac{1}{2} \sum_i \sum_j (C^{-1})_{ij} Q_i Q_j, \tag{4.49}$$

It is important to note that the polarization charge on the capacitor, Q, does not have to be associated with a *discrete* number of electrons, N. This charge is essentially due to a rearrangement of the electron gas with respect to the positive background of ions, and as such it may take on a continuous range of values. It is only when we consider changes in this charge due to the tunneling of a single electron between the conductors that the discrete nature becomes apparent.

Discrete (charge) vs continuous (voltage)

Conditions to observe "quantized effects"

Basic Operation of Single-Electron Box

As the size of the quantum dot decreases, the charging energy W_c of a single exce charge on the dot increases. If the quantum-dot size is sufficiently small and the char ing energy W_c is much greater than thermal energy $k_B T$, no electron tunnels to and fro the quantum dot. Thus, the electron number in the dot takes a fixed value, say zer when both the electrodes are grounded. The charging effect, which blocks the inje tion/ejection of a single charge into/from a quantum dot, is called Coulomb blocka effect. Therefore, the condition for observing Coulomb blockade effects is expressed a

$$W_c = \frac{e^2}{2C} \gg k_B T \ , \qquad ($$

where C is the capacitance of the quantum dot and T is the temperature of the system.

Temperature-related energy fluctuations must be negligible (low T operation!!)

However, it should be noted that by applying a positive bias to the gate electrode w could attract an electron to the quantum dot. The increase of the gate voltage attracts a electron more strongly to the quantum dot. When the gate bias exceeds a certain value a electron finally enters the quantum dot and the electron number of the dot becomes on Further increase of the gate voltage makes it possible to make the electron number tw Thus, in the single-electron box, the electron number of the quantum dot is controlle one by one, by utilizing the gate electrode (Figure 2).

Specific conditions must be fulfilled to realize experimentally the quantum-ruled phenomenon

Conditions for Observing Single-Electron Tunneling Phenomena

In order to observe single-electron tunneling phenomena, or Coulomb blockade effect there are two necessary conditions. One condition is, as described above, that the char ing energy of a single excess electron on a quantum dot is much greater than the therm energy (Eq. (1)). The other condition is that the tunneling resistance R_t of the tunnelir junction must be larger than resistance quantum h/e^2. This condition is required to su press the quantum fluctuations in the electron number, n, of the dot so that they are suff ciently small for the charge to be well localized on the quantum dot. The condition obtained by keeping uncertainty principle $\Delta W \Delta t > h$ while letting ΔW be the chargin energy of the quantum dot, $\sim e^2/C$, and Δt be the lifetime of the charging, $R_t C$. Then, tl uncertainty principle reduces to

$$\Delta W \cdot \Delta t \sim \frac{e^2}{C} \cdot R_t C = e^2 R_t > h \ . \qquad ($$

As a result, one obtains the condition for the tunneling resistance R_t in order to obser the Coulomb blockade effects

$$R_t \gg \frac{h}{e^2} = 25.8 \ \mathrm{k}\Omega. \qquad ($$

Tunneling resistance must be large enough *(weak coupling)*

Da R. Waser Ed., Nanoelectronics and information technology (Wiley-VCH, 2003)

See R. Compaño et al.
MEL-ARI EC Project
Technol. Rodmap 1999

Coulomb blockade (Cb) and SE tunneling

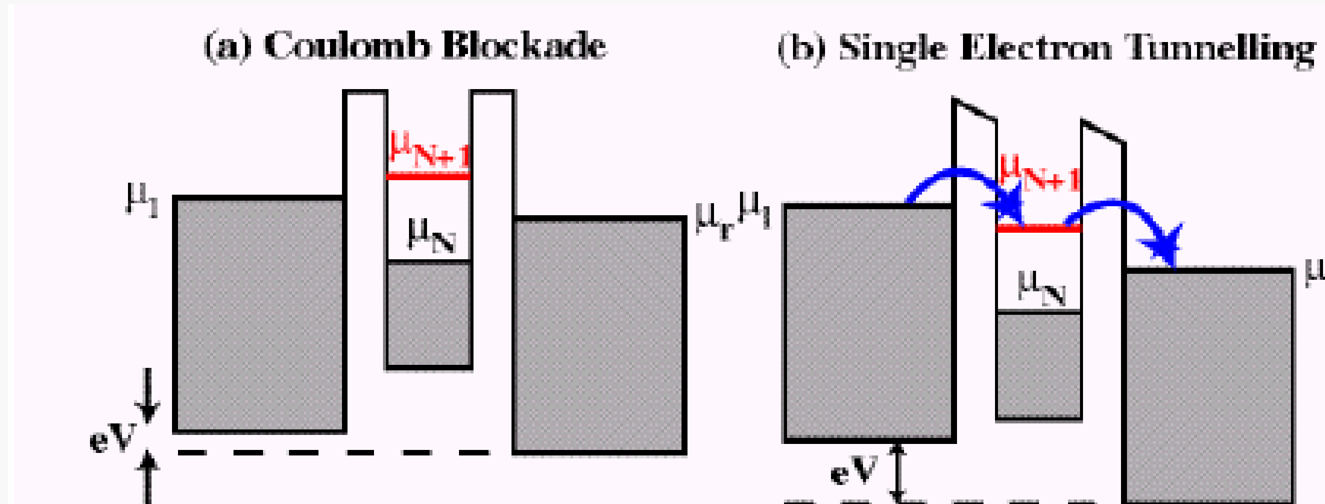

Figure 2.2:- For an island of total capactiance C with N electrons, being μ_N the chemical potential of the highest filled electron state, μ_{N+1} the chemical potential of the first available empty state for an electron and μ_l and μ_r the chemical potentials of the left and right electrodes respectively, it may be shown that the energy to add an electron to the island is $\mu_{N+1}-\mu = e^2/C$. Therefore provided $e^2/C \gg k_BT$ (the thermal energy - i.e. C is small) and the tunnelling resistance, $R_T \gg R_K$ $\approx 25.8k\Omega$ (i.e. the electron wavefunction may be localised on the island) for a voltage V applied across the electrodes, no electrons may flow if $\mu_{N+1} > \mu_l$ and μ_r - the state known as Coulomb blockade (a). If a larger bias is applied across the electrodes such that $\mu_l > \mu_{N+1} > \mu_r$ then empty states may be populated in the island and single electrons may tunnel through the island (b). A gate may be used to change the Fermi level of the island and therefore switch the single electron current on or off.

In quantum mech. terms:

double barrier resonant tunneling

Coulomb blockade: an additional electron is accepted by the dot only if the voltage is raised above some limit

Coulomb oscillations and staircase

Da G. Timp, Nanotechnology (Springer-Verlag, 1999)

After Ferry and Goodnick, Transport in nanostructures, Cambridge (1997)

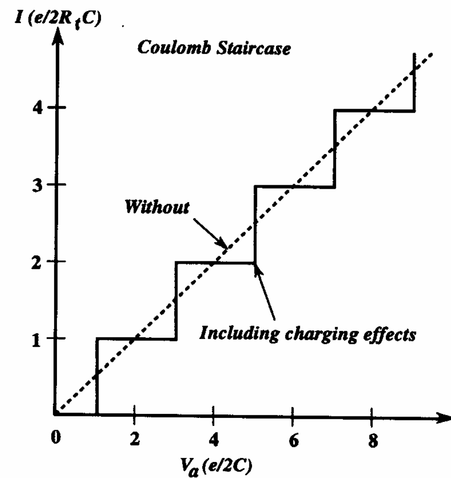

g. 4.15. Ideal current-voltage characteristics for an asymmetric double junction system with and .thout consideration of Coulomb charging effects. For this system, $C_1 = C_2 = C$ and $R_t = R_{t1} \gg$ 2

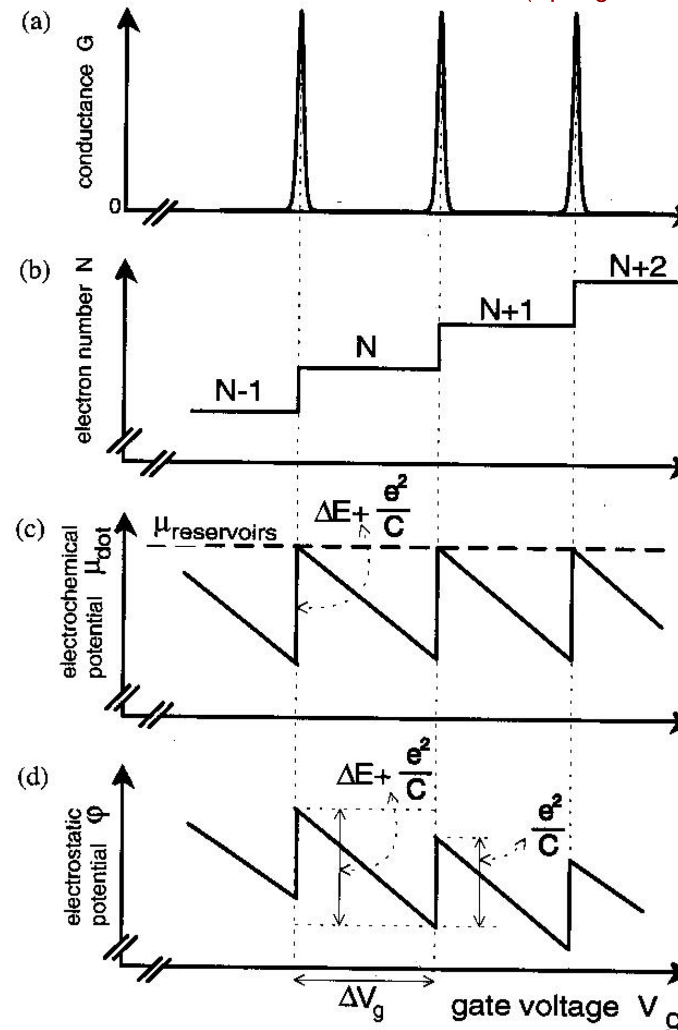

FIGURE 6. Schematic comparison, as a function of gate voltage, between (a) the Coulomb oscillations in the conductance G, (b) the number of electrons in the dot $(N+i)$, (c) the electrochemical potential in the dot, $\mu_{dot}(N+i)$, and (d) the electrostatic potential ϕ.

(Discrete) charge effects inhibit continuous charging of the capacitor, i.e., tunneling transport of electrons through the dot

Examples of measurements

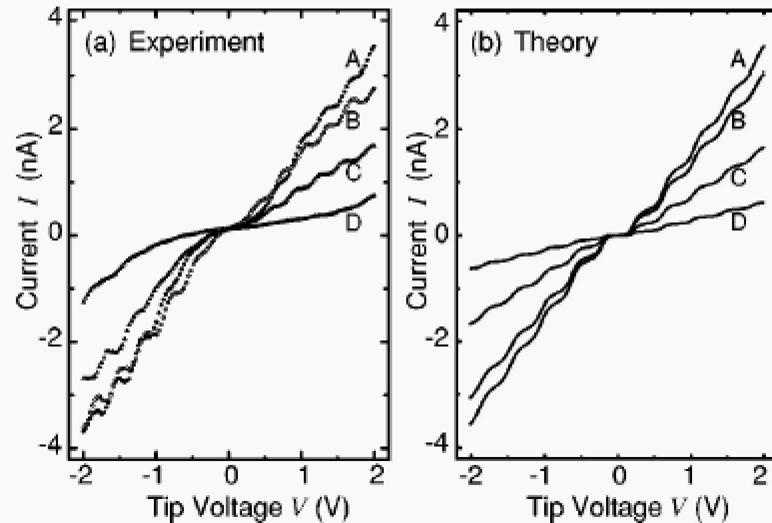

See Imamura et al. PRB 61 46 (2000)

FIG. 3. (a) Experimental I-V curves for a 10-nm-thick $Co_{36}Al_{22}O_{42}$ at room temperature. A, B, C, and D refer to different distances between the STM tip from the surface of the sample. The lateral position for A and B is different from that for C and D. (b) Corresponding theoretical curves in a triple tunnel junction system at $T=300$ K. The tunnel resistance at the bottleneck is taken to be $R_1=600$, 700, 1300, and 3500 MΩ for lines A, B, C, and D, respectively. The other tunnel resistances are $R_2=R_3=1$ MΩ and the capacitances are $C_1=4.48\times10^{-19}$ F, $C_2=2.13\times10^{-19}$ F, and $C_3=3.62\times10^{-19}$ F for all curves.

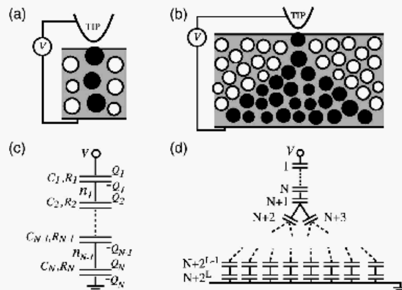

STM measurements
room-temperature
granular metal films
(ø 1-10 nm)

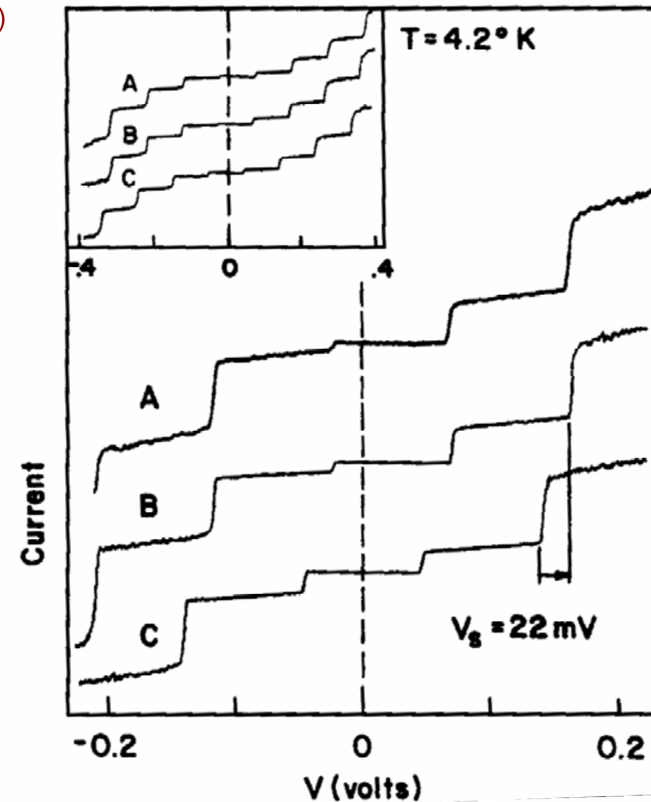

Fig. 4.12. Experimental (A) and theoretical (B and C) I-V characteristics from an STM-contacted 10 nm diameter In droplet illustrating the Coulomb staircase in a double junction system. The peak-to-peak current is 1.8 nA. The curves are offset from one another along the current axis, with the intercept corresponding to zero current. [After Wilkins *et al.*, Phys. Rev. Lett. **63**, 801 (1989), by permission.]

STM used to make a point-like tunneling with nanosized dots

Single Electron Transistor (SET)

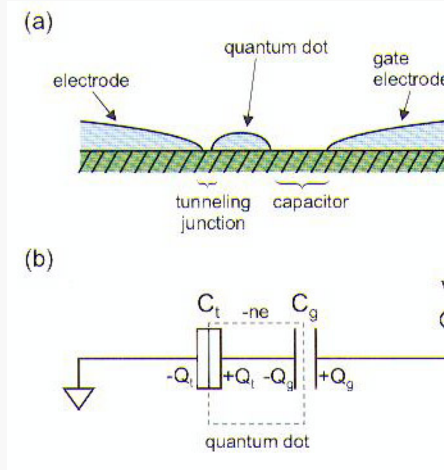

Bias Conditions for Coulomb Blockade Effects

The voltage range, which keeps the electron number at n in the dot, is extracted by con-sidering the free energy of the system. The free energy of the system having n electron in the island $F(n)$ is expressed as

$$F(n)=W_c(n)-A(n)\ ,$$

where $W_c(n)$ is the charging energy and $A(n)$ is the work done by the voltage source co-nected to the gate electrode in order to make the electron number be from zero to n.

It is important to note that when tunneling phenomena do not occur the tunneli junction behaves as a normal capacitor and that the polarization charge on the capacitc does not have to be associated with a discrete number of electrons, n. This polarizati charge is essentially due to a rearrangement of the electron gas with respect to the positive background of ions. Therefore, the polarization charge takes a continuous range of value, although the number of electrons in the quantum dot takes a discrete number of electrons, n. The polarization charges on the tunneling junction and gate capacitor are obtained from the following relationship.

$$Q_t-Q_g=-ne\ ,$$
$$\frac{Q_t}{C_t}+\frac{Q_g}{C_g}=V_g\ , \qquad (5)$$

where Q_t and Q_g are the polarization charge on the tunneling junction and the gate capacitor, respectively. By using Q_t and Q_g, the charging energy $W_c(n)$ of the quantum dot is expressed as,

$$W_c(n)=\frac{Q_t^2}{2C_t}+\frac{Q_g^2}{2C_g}\ , \qquad (6)$$

which reduces to

$$W_c(n)=\frac{e^2n^2}{2C_\Sigma}+\frac{1}{2}\frac{C_tC_gV_g^2}{C_\Sigma}\ , \qquad (7)$$

where $C_\Sigma = C_t + C_g$. In addition, the work, $A(n)$, done by the gate voltage source in order to make electron number of the quantum dot be from zero to n is expressed as,

$$A(n)=\int I(t)\cdot V_g dt=Q_gV_g=en\frac{C_g}{C_\Sigma}V_g+\frac{C_tC_gV_g^2}{C_\Sigma}\ . \qquad (8)$$

In order to maintain the electron number in the quantum dot, the following conditions are required.

$$F(n)<F(n\pm1) \qquad (9)$$

From Eqs.(7) to (9), the voltage range, within which Coulomb blockade effects are in effect and the electron number of the dot takes a fixed value of n, can be obtained as follows.

$$\left(n-\frac{1}{2}\right)\frac{e}{C_g}<V_g<\left(n+\frac{1}{2}\right)\frac{e}{C_g} \qquad (10)$$

This condition is also expressed with critical charge Q_c as follows.

$$|Q|<Q_c\ , \qquad (11)$$

where Q_c is expressed as,

$$Q_c=\frac{e}{2}\left(1+\frac{C_g}{C_t}\right)^{-1}\ . \qquad (12)$$

Free energy change $\Delta F(n, n+1)$ that accompanies a transition of the electron number from n to $n+1$ is also simply expressed with critical charges Q_c as,

$$\Delta F(n,n+1)=F(n+1)-F(n)=\frac{e}{C_t}(Q_t-Q_c)\ . \qquad (13)$$

SET operation (in electronic terms)

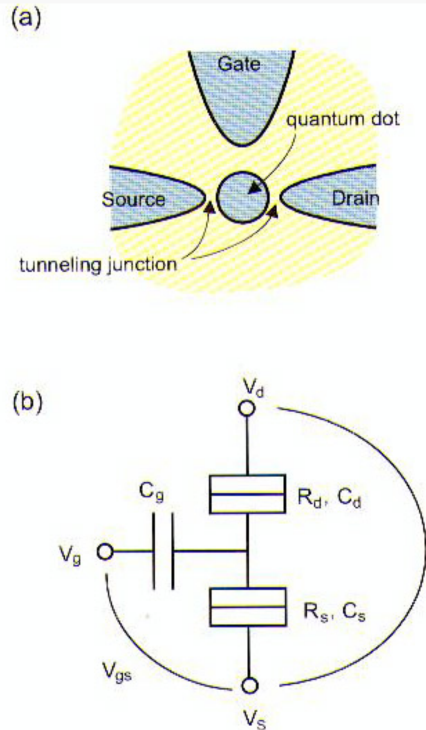

Figure 3:
(a) Schematic structure of single-electron transistor.
(b) Equivalent circuit of single-electron transistor.

Operation of Single-Electron Transistors

The operation of single-electron transistors can be described by using Thévenin's theorem and applying derived Eqs. (10) - (12) for a single-electron box.

By using the Thévenin's theorem, the circuit connected to the tunneling junction of the source is transformed to the circuit shown in Figure 4a. From this equivalent circuit and Eq. (10), the condition to maintain the electron number at n in the dot is expressed as

$$\left(n-\frac{1}{2}\right)\frac{e}{C_g+C_d}<\frac{C_gV_g+C_dV_d}{C_g+C_d}<\left(n+\frac{1}{2}\right)\frac{e}{C_g+C_d}\ , \tag{14}$$

which reduces to

$$\frac{1}{C_d}\left(ne-\frac{e}{2}-C_gV_g\right)<V_d<\frac{1}{C_d}\left(ne+\frac{e}{2}-C_gV_g\right)\ . \tag{15}$$

In the same manner, the circuit connected to the tunneling junction of the drain is transformed to the circuit shown in Figure 4b and the condition to maintain the electron number at n in the dot is expressed as

$$\frac{1}{C_s+C_g}\left(-ne+\frac{e}{2}+C_gV_g\right)>V_d>\frac{1}{C_s+C_g}\left(-ne-\frac{e}{2}+C_gV_g\right) \tag{16}$$

Figure 5a shows the relationship between the drain voltage V_d and the gate voltage V_g, which satisfies the conditions expressed by Eqs. (15) and (16). The gray areas shown in Figure 5a are Coulomb blockade regions, where the Coulomb blockade is effective and the electron number in the dot takes a fixed value indicated in the areas.

On the other hand, in other regions, the quantum dot can take at least two electron numbers. In the green regions shown in Figure 5a the quantum dot can take two electron numbers. For example, in the green region indicated by A, the electron number in the dot is zero or one. More precisely, the electron number of one is preferable for the tunneling junction of the source and the electron number of zero is preferable for the tunneling junction of the drain. Therefore, when a finite positive source-to-drain voltage V_{ds}, indicated by dashed line in Figure 5a, is applied between the source and drain electrodes and the gate voltage is $e/2C_g$, an electron transport process described below is observable. The initial electron number of the dot is assumed to be zero. For the tunneling junction of the source, the electron number of one is preferable so that an electron tunnels from the source to the dot and the electron number in the dot becomes one. However, for the tunneling junction of the drain, the electron number of zero is preferable so that an electron tunnels from the dot to the drain and the electron number in the dot becomes zero. As a result, an electron tunnels from the source to the drain, and source-to-drain current is observable at these bias conditions.

In the same manner, at the gate voltage of $ne/C_g + e/2C_g$, the source-to-drain current I_{ds} is observed, and thus oscillating I_{ds} versus V_g characteristics shown in Figure 5b is observed in single-electron transistors. The oscillating I_{ds} - V_g characteristics are called Coulomb oscillations.

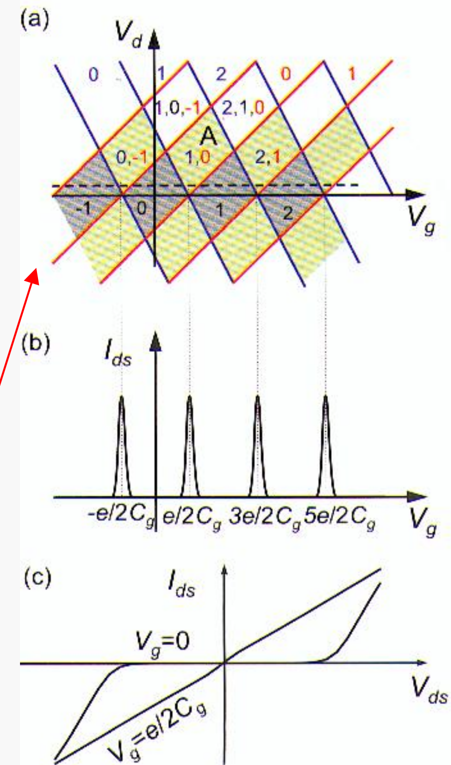

Figure 5:
(a) Relationship between the drain voltage V_d and the gate voltage V_g, satisfying the conditions expressed by Eqs. (15) and (16). The diamond-shaped structure along the x-axis is called Coulomb diamond.
(b) source-to-drain current I_{ds} versus gate voltage V_g characteristics of single-electron transistors.
(c) I_{ds} versus V_{ds} characteristics of single-electron transistors.

A gate is added to change the voltage, i.e., to control the tunneling through the dot

(Unconventional) practical implementations

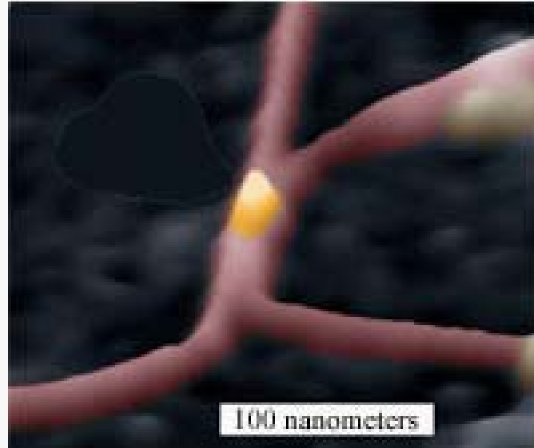

A tiny speck of gold positioned between two parallel carbon nanotubes forms a transistor that forwards one electron at a time. These single electron transistors could be used to make extremely small, low-power logic circuits.

Source: Lund University

See Thelander and Samuelson Nanotechnology 13 108 (2002)

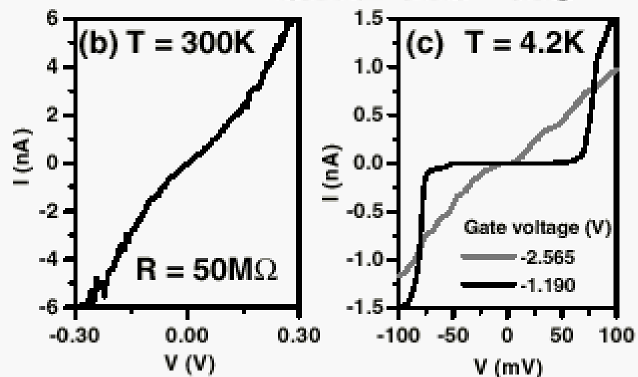

Produced by **scanning probe manipulation** of small metal dots

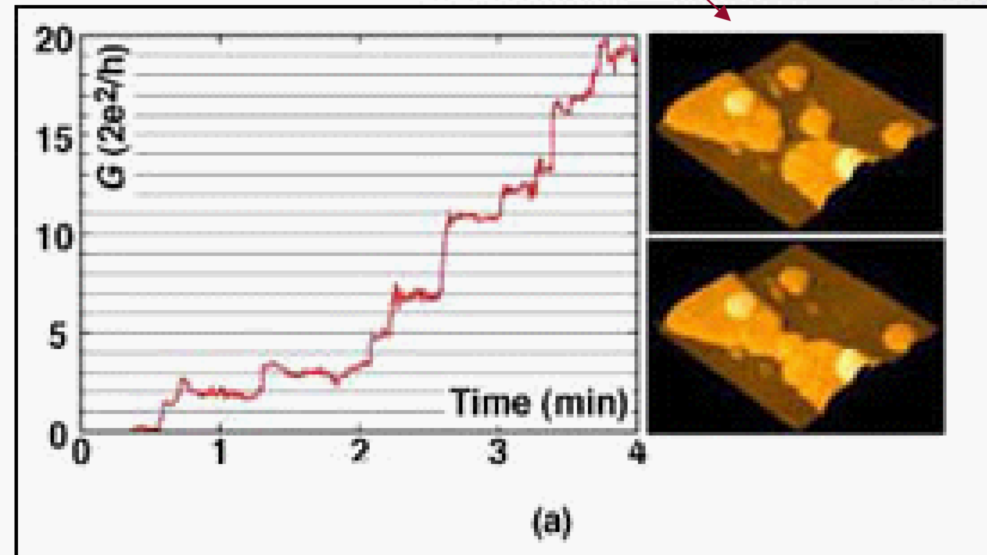

See Junno et al., APL 72 548 (1998); APL 80 (2002)

SET advantages (for the electronics)

Scaling down of electronic device sizes has been the fundamental strategy for improving the performance of ultra-large-scale integrated circuits (ULSIs). Metal-oxide-semiconductor field-effect transistors (MOSFETs) have been the most prevalent electron devices for ULSI applications, and thus the scaling down of the sizes of MOSFETs [1][2] has been the basis of the development of the semiconductor industry for the last 30 years.

However, in the early years of the 21st century, the scaling of CMOSFETs is entering the deep sub-50 nm regime [3]. In this deep-nanoscaled regime, fundamental limits of CMOSFETs and technological challenges with regard to the scaling of CMOSFETs are encountered [4]. On the other hand, quantum-mechanical effects are expected to be effective in these small structured devices. Therefore, in order to extend the prodigious progress of LSI performance, it is essential to introduce a new device having an operation principle that is effective in smaller dimensions and which may utilize the quantum-mechanical effects, and thus provide a new functionality beyond that attainable with CMOSFETs.

Single-electron devices [5][6] are promising as new nanoscaled devices because single-electron devices retain their scalability even on an atomic scale and, moreover, they can control the motion of even a single electron. Therefore, if the single-electron devices are used as ULSI elements, the ULSI will have the attributes of extremely high integration and extremely low power consumption. In this respect, scalability means that the performance of electronic devices increases with a decrease of the device dimensions. Power consumption is roughly proportional to the electron number transferred from voltage source to the ground in logic operations. Therefore, the utilization of single-electron devices in ULSIs is expected to reduce the power consumption of ULSIs.

On the other hand, as for the disadvantages, 1) operations of SET circuits are generally limited to low temperature. This is a negative aspect of the good scalability. In order to operate SET circuits at room temperature, the size of the quantum dot must be much smaller than 10 nm. With the present technology, fabricating a structure smaller than 10 nm is difficult. In addition, 2) SETs have the disadvantage of high output impedance, due to the high resistance of tunnel junctions, which must be much higher than 25.8 kΩ (Eq. (3)). Finally, 3) source-to-drain voltage of SETs should be smaller than gate voltage swing in order to use SETs as gate controlled switching device, because the potential of the dot is easily affected by the source-to-drain voltage. The effect of source-to-drain voltage on the switching characteristics of SETs will be quantitatively evaluated in Sect. 3.2.

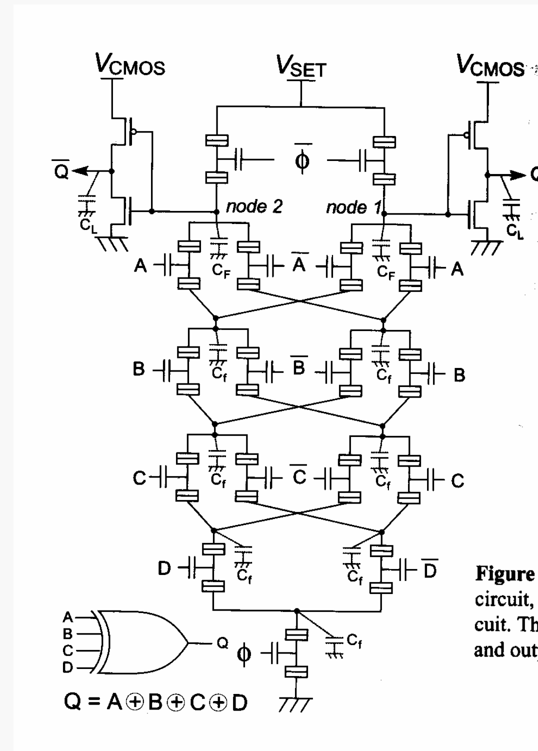

Figure 20: Example of SET logic circuit, four-way exclusive OR circuit. The complementary imputs and outputs are used.

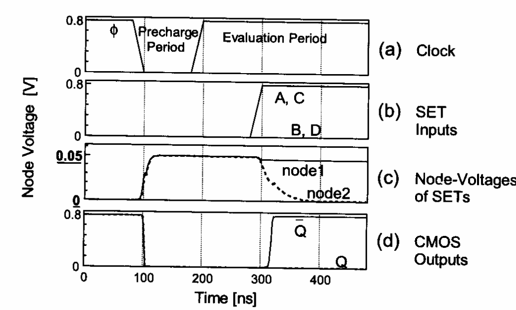

Figure 21: The simulated timing chart of the circuit shown in Figure 20. Here, $C_g = 0.1$ aF, $C_s = C_d = 0.06$ aF, $R_t = 500$ kΩ, $C_L = 10$ fF, $C_F = 1$fF, $C_f = 50$ aF, $V_{SET} = 50$ mV, and $T = 293$ K.

Example of mixed SET/CMOS technology

Quantum dot / quantum well

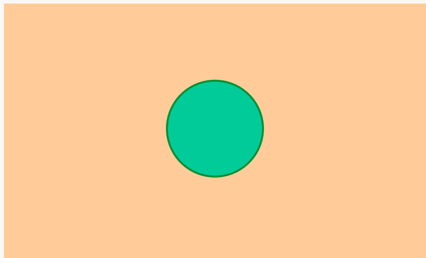

A nanosized dot embedded in the "outer" world is a 3D quantum well (spherical quantum box)

Simple 1D case

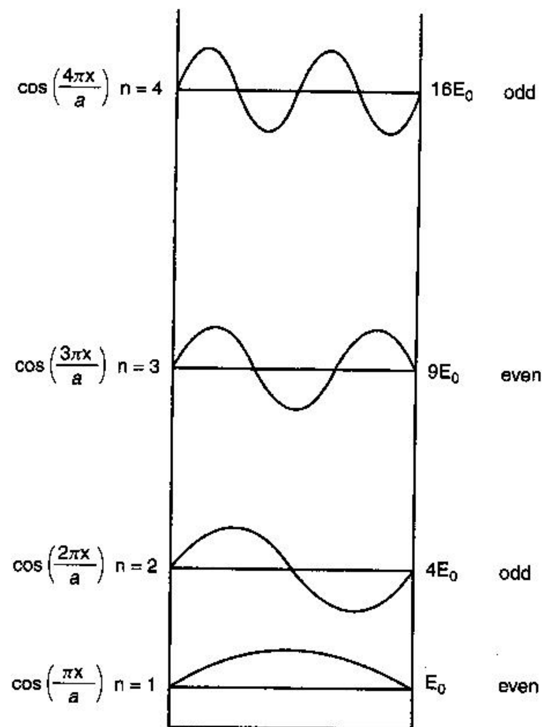

Figure 9.11. Sketch of wavefunctions for the four lowest energy levels ($n = 1$–4) of the one-dimensional infinite square well. For each level the form of the wavefunction is given on the left, and its parity (even or odd) is indicated on the right (From C. P. Poole, Jr., *Handbook of Physics*, Wiley, New York, 1998, p. 289.)

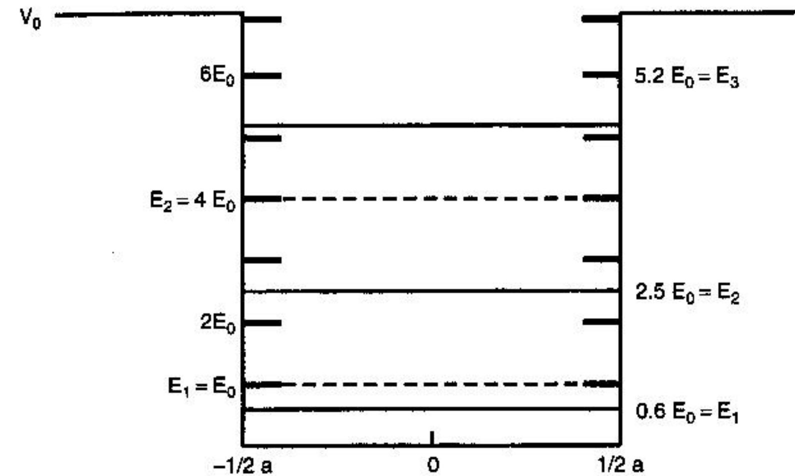

Figure 9.12. Sketch of a one-dimensional square well showing how the energy levels E_n of a finite well (right side, solid horizontal lines) lie below their infinite well counterparts (left side, dashed lines). (From C. P. Poole, Jr., *Handbook of Physics*, Wiley, New York, 1998, p. 285.)

Effects relevant in optical properties (already seen) may have a counterpart in electron wavefunction behavior

ens
notechn.

Size, barrier height, material and energy

A “**material discontinuity**” is needed to define the well, e.g.: metal/vacuum, metal/oxide, semiconductor/oxide, **semiconductors with different gap energies**

In the actual conditions, the potential barrier is finite, but *few differences with respect to infinite case* (possibility of tunnelling, slight change in level energy, typically a few excited levels can be kept in the well, …)

Punti quantici (Q.D.). La nanostruttura più difficile da ottenere, ma anche la più complessa per i suoi effetti sulle proprietà ottiche e di trasporto, è quella in cui il confinamento del materiale a “gap” inferiore avviene in tutte e tre le direzioni dello spazio. Dal punto di vista della simmetria di traslazione si può allora dire che la struttura è a dimensionalità zero, e per questo viene chiamata “punto quantico” (Q.D. dall'inglese Quantum Dot). I livelli di energia per gli elettroni e per le buche sono solo livelli discreti, risultanti dal confinamento. Si può ottenere una prima grossolana approssimazione per gli elettroni dal calcolo quantistico degli stati della buca cubica a pareti infinite di lato L,

$$E_{n_x,n_y,n_z} = E_g + \frac{\pi^2\hbar^2}{2m^*L^2}(n_x^2+n_y^2+n_z^2), \qquad (11.92)$$

con $(n_x, n_y, n_z = 1, 2, \ldots)$. Si ottiene un simile risultato per le buche, con la separazione tra stati di massa pesante e di massa leggera dovuti al confinamento. Il calcolo preciso, con potenziale finito, richiede anche in questo caso l'uso delle condizioni di continuità al contorno e lo sviluppo della matrice di Luttinger per le buche.

Simple one dimensional case

$E_n = \hbar^2 k_n^2 / (2\, m^*)$ with $k_n = n\, 2\pi / L$

$$\mathbf{E_n = n^2 \hbar^2 \pi / (2\, m^*\, L^2)}$$

material (→ m^*), *size* (→ L)

$$\mathbf{\Delta E_n = (2n + 1)\, \hbar^2 \pi / (2\, m^*\, L^2)}$$

Level energies can be “engineered”

Example: free electron (m_e), width L=5 nm: $E_{n=2} - E_{n=1} \sim 1$ eV (even larger for electrons in a semiconductor if $m^* < m_e$)

Semiconductor quantum dots and SET

Semiconductor Quantum Dot

It should be noted that when the quantum-dot size is comparable with the de Broglie wavelength of the electrons in quantum dots (this situation frequently occurs in the case of semiconductor nanoscaled quantum dots), the energy quantization becomes comparable with the charging energy. In this case, the energy difference due to the addition of a single electron to the dot is given not by the charging energy W_c but by the electron addition energy W_a, which is given by the following formula.

$$W_a = W_c + \Delta W \qquad (22)$$

Here ΔW is the quantum energy level difference due to the addition of a single electron to the dot.

As a result, periodicity of Coulomb oscillations is modified as [10],

$$\Delta V_g = \frac{e}{C_g} + \frac{\Delta W}{e} \,. \qquad (23)$$

Thus, in quantum dots holding just a few electron, the electron addition energy W_a can no longer parameterized with W_c, and the Coulomb oscillations are significantly modified by electron-electron interactions and quantum confinement effects. Therefore, in this case, quantum dots are regarded as *artificial atoms* [14].

By utilizing Eq. (23), the energy spectrum of a quantum dot, or an *artificial atom*, can be studied. Tarucha *et al.* have fabricated vertical single-electron transistors (SETs) having circular-disk-shaped dots with double heterostructure barriers and surrounding side gate, shown in Figure 6, and observed, in the transport measurements, atom-like properties such as "magic numbers" and "Hund's first rule" [15], [16], [17].

In the vertical SET, the quantum dot is located in the center of the pillar. The diameter of the dot is a few hundred nanometers and its thickness is about 10 nm. The dot is sandwiched with two non-conducting heterostructure barrier layers, which separate it from conducting material above and below. A negative voltage applied to the side gate around the pillar squeezed the effective diameter of the dot. Consequently, the number of electrons is reduced, one by one, until the dot is completely empty.

If the lateral confinement has the form of harmonic potential, the eigen-energy $W_{n,l}$ is expressed with radial quantum number n_r (=0, 1, 2, …) and the angular momentum quantum number l (= 0, ±1, ±2, …):

$$W_{n_r,l} = \left(2n_r + |l| + 1\right)\hbar\omega_0 \,, \qquad (24)$$

where $\hbar\omega_0$ is the lateral confinement energy [16], [17]. Here, the Zeeman effect is neglected. Therefore, it should be noted that each state is spin degenerate.

Vertical SET

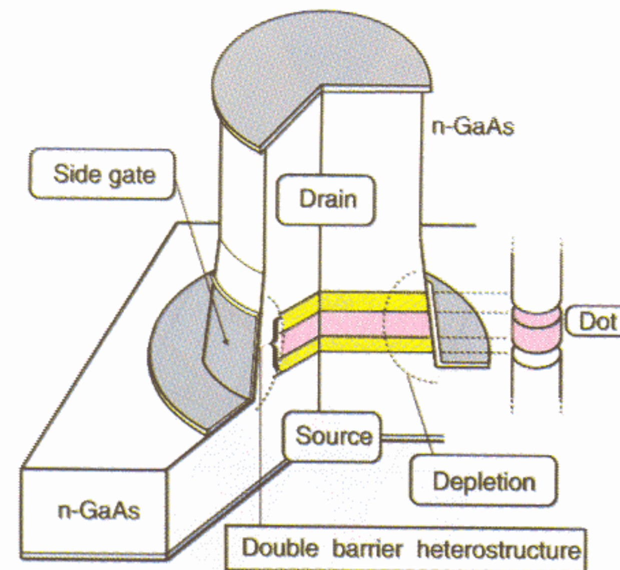

Figure 6: Schematic of a quantum dot in a vertical device (After Tarucha *et al.* [17], © 2001 IOP Publishing Co.).

Artificial atom in vertical SET

Figure 7a shows the I_d - V_g characteristics, or Coulomb oscillation characteristics, of the vertical SET. The distance between the consecutive peaks is proportional to W_a, which is the energy difference between the transition point of (N to $N+1$) and ($N+1$ to $N+2$) electrons and is equal to the difference of the ionization energy and the electron affinity [18]. The addition energies, W_a's, extracted form the I_d - V_g characteristics are summarized in the inset of Figure 7a. It should be noted that W_a is not constant, and larger energy is necessary to add an electron to the dot with 2, 6, and 12 electrons. The numbers in this sequence can be regarded as "magic numbers" for a two-dimensional harmonic potential dot [15].

The reason is explained as follows [15], [16], [17]. Figure 7b shows the two-dimensional orbits allowed in the dot. The orbit with the smallest radius corresponds to the lowest energy state ($W_{0,0}$), which has zero angular momentum and can have two electrons with opposite spin. The addition of the second electron thus only costs the charging energy, e^2/C. Extra energy ΔW is necessary to add the third electron, because the electron must go into the next energy state ($W_{0,-1}$, $W_{0,1}$), which has an angular momentum ± 1 and can have four electrons. Therefore, extra energy is again necessary to add the seventh electron. The numbers in the above sequence can be thus regarded as *magic numbers* for a two-dimensional harmonic dot.

In addition, for the filling of electrons in the same orbit, parallel spins are favored by "Hund's first rule". This leads to another series of magic numbers of N = 4, 9, 16, … corresponding to the half filling of the second, third, fourth orbits, respectively [17].

Thus, the atomic-like features are successfully observed in the vertical SETs having circular disk quantum dots.

Since the above discussions concerning artificial atoms are based on ref. [16], [17], the interested reader is advised to refer to the original monographs [16], [17] and related articles, such as [15], [19], [20].

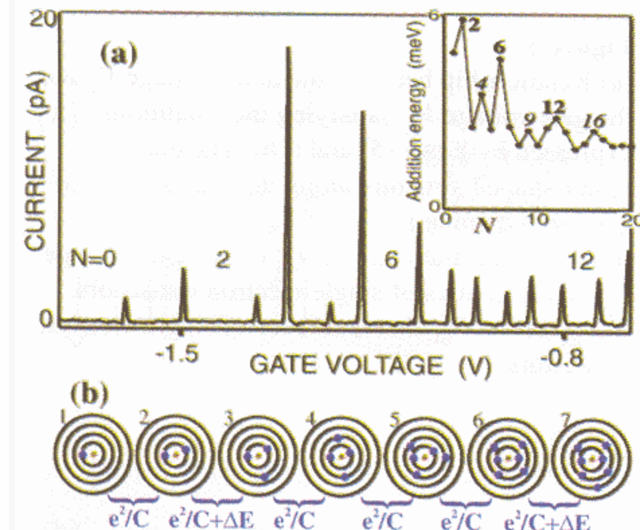

Figure 7: Current flowing through a two dimensional circular quantum dot on varying the gate voltage.
(a) The first peak marks the voltage where the first electron enters the dot, and the number of electrons, N, increases by one at each subsequent peak. The distance between adjacent peaks corresponds to the addition energies (see inset).
(b) The addition of electrons to circular orbits is shown schematically. The first shell can hold two electrons whereas the second shell can contain up to four electrons. It therefore costs extra energy to add the third and seventh electrons (After Kouwenhoven *et al.* [16], © 2001 IOP Publishing Co.).

Artificial atom-like behavior achieved in specific quantum dot configurations

SET fabrication (conventional): example I

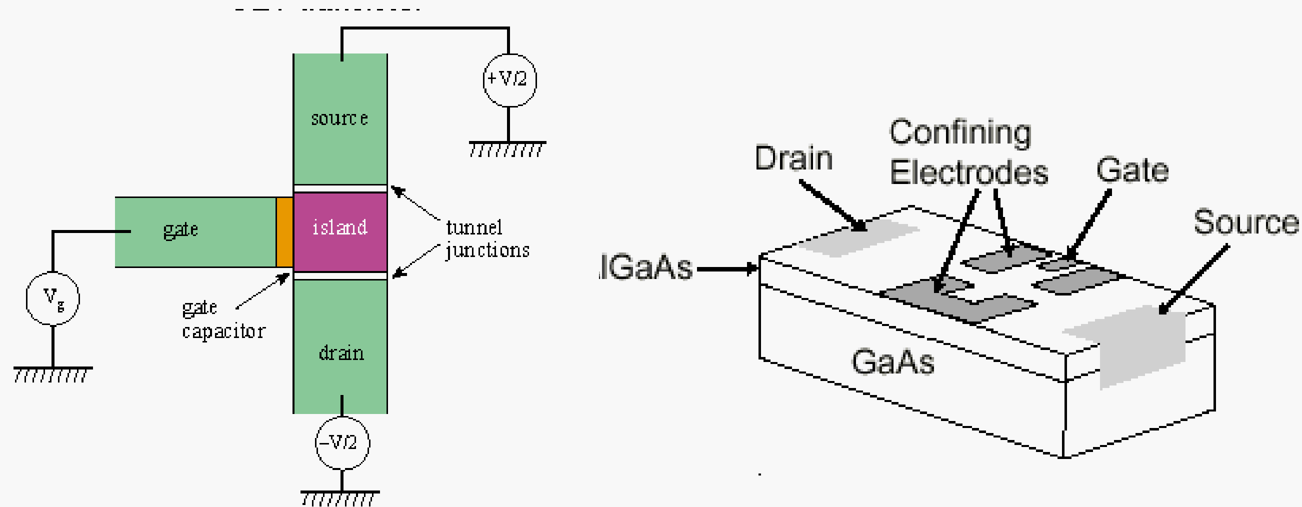

See Kastner
Ann.Phys 9 885 (2000)

Fig. 1 Schematic drawing of a SET. Wires are connected to source and drain contacts to pass current through the 2DEG at the GaAs/AlGaAs interface. Wires are also connected to the confining electrodes to bias them negatively and to the gate electrode that controls the electrostatic energy of the confined electrons.

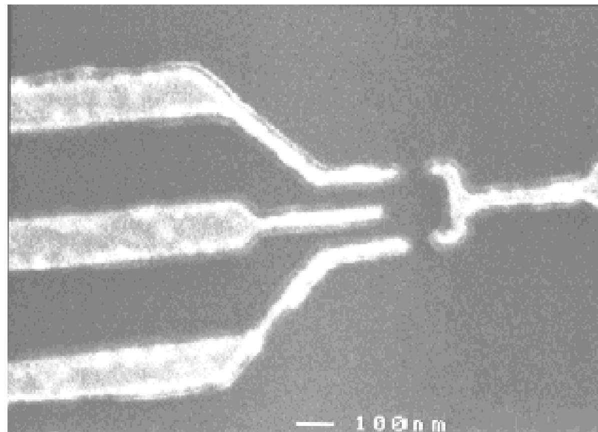

SET: three-terminal device similar to MOSFET but:
single electron capabilities, high speed (ps range), no consumption *(but requires low T!!)*

SET fabrication (conventional): example II

!.4 Fabrication of Single-Electron Devices

'here have been a number of reports on the fabrication of single-electron devices. Since ingle-electron phenomena can be observed in any conductive substances, single-elec- ron devices are fabricated in a variety of materials such as aluminum [24], heterostruc- ures [25], and silicon. However, in order to utilize single-electron devices as elemental levices of LSIs, the realization of single-electron devices made in silicon is essential. 'his can be achieved if fabrication techniques of nanometer-scaled silicon quantum dots re established.

Regarding silicon quantum dot formation, many approaches have been reported 26], [27], [28], [29], [30], [31] and they are generally categorized into two groups: pat- erning the silicon quantum dots by fine-lithography techniques and the growth of sili- on quantum dots by deposition processes.

Using the former approaches, it is possible to accurately define the structures and ositions of quantum dots. For example, Takahashi *et al.* proposed a novel silicon-quan- um-dot fabrication process named pattern-dependent oxidation (PADOX) [26]. When a -D Si nano-wire, which has wide 2-D Si layers at its ends and is fabricated in sili- on-on-insulator (SOI) wafer, is subjected to oxidation process, the oxidation process ot only reduces the width and height of the 1-D Si wire, but also constricts the Si wire at its ends. Since oxygen atoms penetrate not only from the surface oxide layer but also from the backside (the interface of SOI and buried oxide) through the pattern side, oxi- dation occurs more in the neighborhood of the pattern edges of the 2-D Si layers, as shown in Figure 8. Ono *et al.* have developed the vertical version of PADOX (V-PADOX) [27], shown in Figure 9. In PADOX, laterally broad 2-D regions are essen- tial for tunnel-barrier formation. On the other hand, in V-PADOX, vertically broad, namely thick, 2-D regions are utilized for the tunnel-barrier formation. The advantage of the V-PADOX is that the V-PADOX makes it possible to form two tiny islands in a small area by utilizing not a lithographic process but the oxidation process, which induces the accumulation of stress in small structures. Thus, by utilizing V-PADOX, two SETs can be fabricated in an extremely small area, as shown in Figure 10.

The latter approaches are favorable from the viewpoints of throughput and fabri- cated quantum-dot sizes. In fact, Yano *et al.* successfully fabricated the room-tempera- ture operating silicon single-electron memory by using the formation process of thin poly-silicon film, in which an array of 10-nm grains is naturally formed [28]. Tiwari *et al.* reported single-electron memory having Si nanocrystal storage [29].

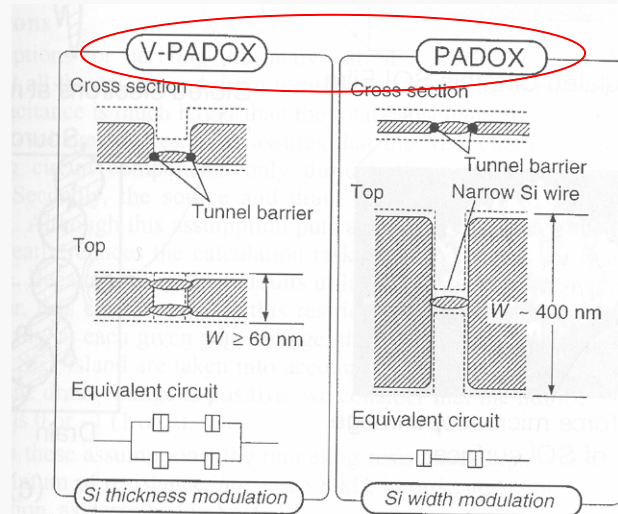

Figure 9: Si patterns and the corresponding circuits for V-PADOX and PADOX. In the cross-sectional and top views, broken lines represents preoxidation Si patterns and hatched regions represent islands and leads after oxidation (After Ono *et al.* [27], © 2000 IEEE).

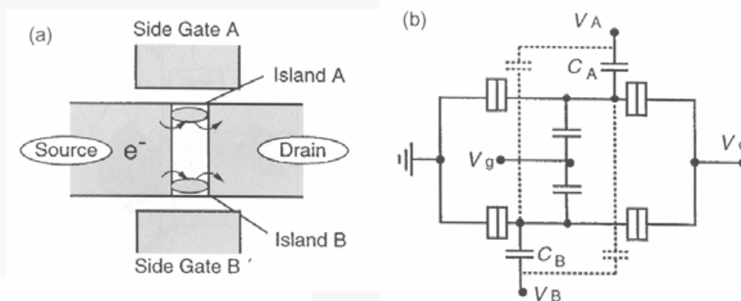

Figure 10: Fabrication of two SETs.
(a) Top view of the structure.
(b) Equivalent circuit (After Ono *et al.* [27], © 2000 IEEE).

(Anisotropic) oxidization used to obtain Si quantum dots

SET fabrication (conventional): example III

Uchida *et al.* proposed another approach, where slight etching of an ultrathin SOI film with an alkaline-based solution is utilized [30], [32]. The proposed device structure is schematically illustrated in Figure 11a. As shown in the figure, the device structure is almost the same as that of conventional SOI-MOSFETs, but the SOI film has two key features: 1) its surface is intentionally undulated in nanoscaled dimensions as shown in Figure 11b by utilizing an alkaline-based solution; 2) the channel SOI thick-ness is thinned to a few nanometers. The nanoscaled undulation in the ultrathin film results in the formation of nanoscaled potential fluctuations due to the difference of quantum confinement effects from one part to another. Consequently, both the narrow electron channel through potential valleys and small potential pockets, storing memory information, are formed in the film as shown in Figure 11c. Since potential fluctuation still exists in the narrow channel, the channel effectively splits into several quantum dots. The quantum dots included in the channel are the origin of the SET operation. Thus, the device works as a single-electron transistor with nonvolatile memory function. Since the fabrication process of this SET is compatible with that of CMOSFETs. SET/CMOS hybrid circuit is fabricated on a chip, as shown in Figure 12, and its operation is successfully demonstrated even at room temperature [32].

Nanosized "undulation" (obtained by mild etching) leads to a sequence of quantum dots

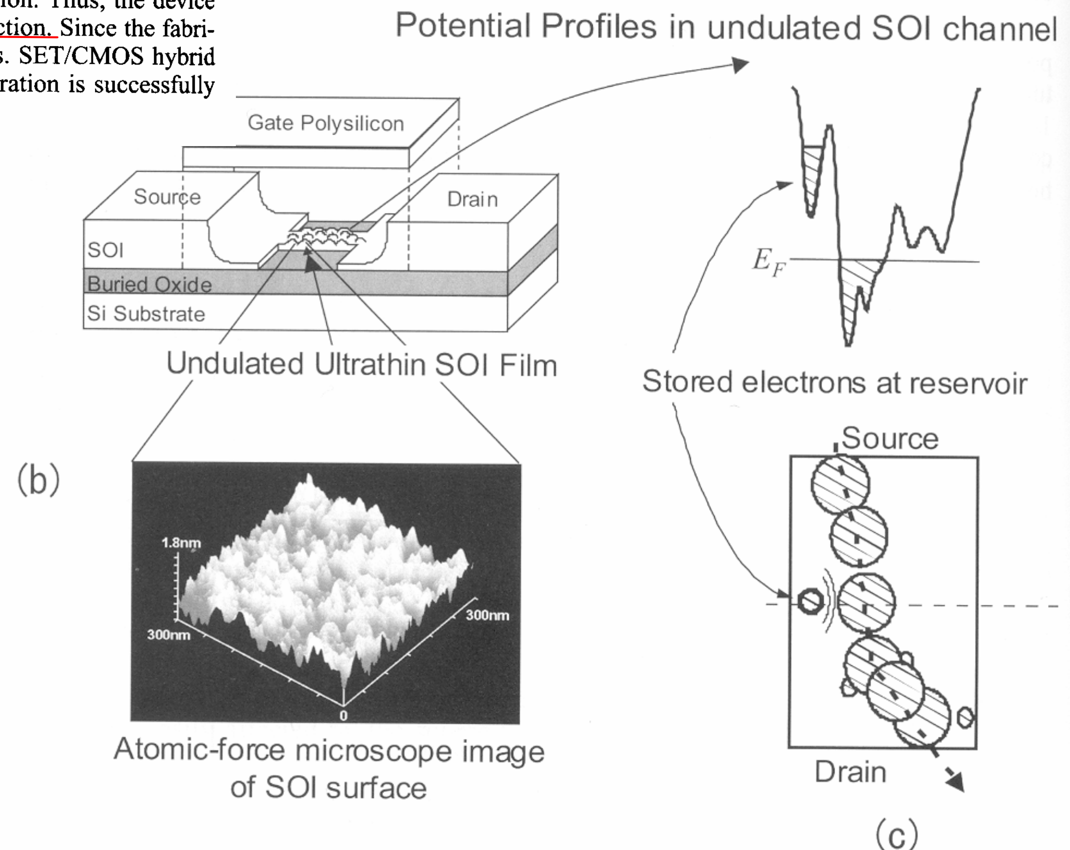

Figure 11: Device structure and operation principle of single-electron transistor with nonvolatile memory function.

Tunneling through quantum dots

Da R. Waser Ed., Nanoelectronics and information technology (Wiley-

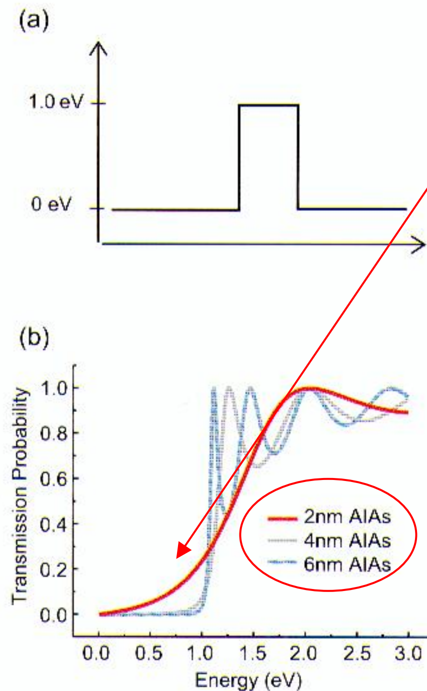

Figure 2: Schematic band diagram of a single AlAs barrier (a) and the correspond-ing tunneling transmission probability for different barrier thicknesses (b).

2.1.1 Tunneling Through a Single Barrier

We consider the tunneling probability through a single potential barrier Figure 2. The experimental equivalent is an AlAs barrier embedded in GaAs. The electron transmission probability as a function of the electron energy was calculated according to Eq. (15) for three different thicknesses of the barriers. First we observe a finite transmission probability for electrons far below the potential height of 1.0 eV. This effect is known as the tunneling effect. The electron wave function in front of the barrier leaks out through the barrier and leads to a finite transmission. The smaller the barrier thickness, the higher is the tunneling probability of the electrons with energies below the potential energy of the barrier. In a classical picture the electrons could not penetrate the barrier. In addition we see a modulation of the transmission probability for electrons at energies above the 1.0 eV barrier height. In this region interference effects of transmitted and reflected electron waves appears, which demonstrate the wave character of the electrons.

2.1.2 Tunneling Through a Double Barrier Structure

To see the difference between the tunneling effect through a single barrier and the resonant tunneling effect, we discuss the case of a double barrier structure (see Figure 3). We consider two 4 nm thick AlAs barriers separated by a 5 nm GaAs well. In contrast to the transmission through a single barrier now electrons with very low energies can cross the double barrier structure with a transmission probability of 1. Three additional very sharp maxima appear below 1 eV in Figure 3b: they could be interpreted as quasi-bound states with a very narrow energetic bandwidth, through which electrons can tunnel like

through open channels in the barrier. This is at first astonishing and not compatible with a sequential tunneling picture. In a sequential transport picture we would expect that the transmission probability through two barriers is very much smaller than through one barrier because the transmission through the first barrier is already much below 1. A completely new quantum mechanical system has been developed which can not be described by the behaviour of each single system. This may also be a drawback for quantum devices in general. Quantum mechanical devices can therefore not be placed extremely close to each other without changing the characteristics of the single device.

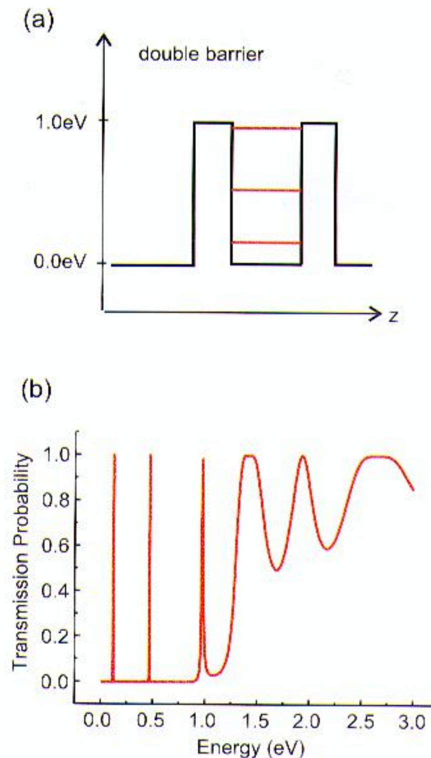

Figure 3: Schematic band diagram of a double barrier structure of AlAs embedded in GaAs (a) and the corresponding tunneling transmission probability (b).

Single barrier

"Resonances" may appear corresponding to the positions of the quantum dot energy levels

Double barrier

Resonant Tunneling Diode (RTD) I

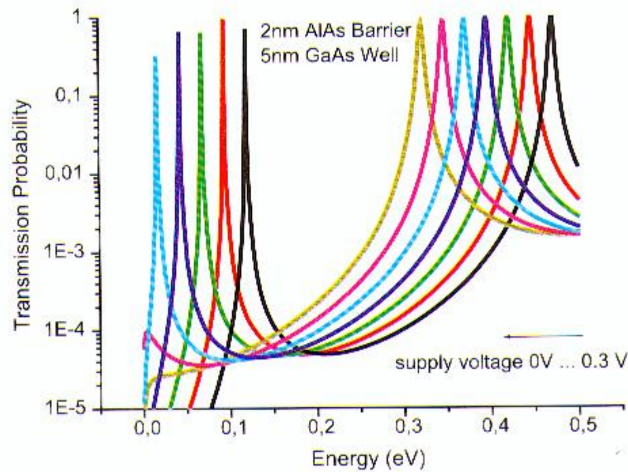

Figure 5: Transmission probability of a double barrier structure at different supply voltages.

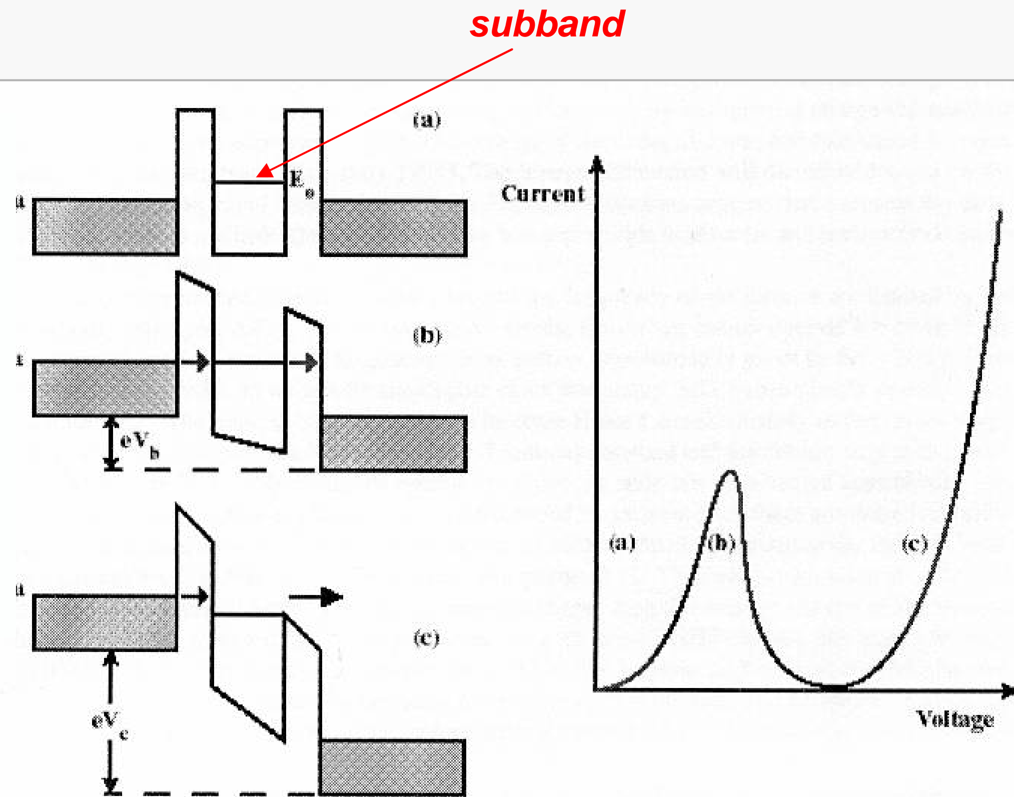

Figure 2.3:- Basic concept of the RTD. The subband energy Eo is approximately inversely proportional to the square of the well thickness. The peak in the I-V curve occurs when the incident electrons match the energy of the subband and the electrons resonantly tunnel from the source to the drain.

RTD proposed as a system with extremely high speed and low consumption

Resonant Tunneling Diode (RTD) II

3.2 Current-Voltage Characteristics

The current density at a certain supply voltage can be calculated using the transmission probability together with the corresponding actual electron occupation densities. For the example of a double barrier structure the highly doped supply layers left and right of the double barrier can be described as free electron gases. The current density is obtained as the difference between the current density flux from the left to the right side of the double barrier and that one in the opposite direction. After Tsu *et al.* [2] this can be written as:

$$j=\frac{2|e|}{(2\pi)^3}\int_0^\infty dk_z\int_0^\infty dk_\parallel\big(f_l(W)-f_r(W+eV)\big)T_c(W_z,V)\frac{1}{\hbar}\frac{\partial W_z}{\partial k_z} \tag{18}$$

where the coherent transmission probability $T_c(W_z,V)$ is a function of the supply voltage V and energy in z direction W_z, f_l and f_r are the Fermi distributions, left and right of the double barrier, and $k_\parallel$ and k_z denote the parallel- and z-component of the momentum, respectively. The integration of Eq. (18) leads to the current density expression containing the supply function:

$$j(V)=\frac{4\pi|e|m^*k_BT}{h^3}\int_0^\infty dW_zT_c(W_z,V)\ln\left|\frac{1+\exp\left(\frac{W_F-W_z}{k_BT}\right)}{1+\exp\left(\frac{W_F-W_z-eV}{k_BT}\right)}\right| \tag{19}$$

For an accurate calculation of the transmission probability the real potential profile across the device is required. The potential Φ includes the device energy band offset of the heterojunctions, the voltage drop across the structure and the contributions from the doping and mobile charges. By coupling the effective mass Schrödinger equation with the Poisson equation the potential Φ is obtained in a self-consistent manner.

Calculations of current voltage characteristics lead to a deeper insight into the physics of resonant tunneling diodes and are necessary in the device designing. A typical calculation is shown in Figure 6. The main characteristic feature is the existence of a negative differential resistance region which is the base of most of the RTD-applications. From the application point of view important parameters are: the peak current density, the valley current density, the peak to the valley current density ratio (PVR) and the peak voltage.

The peak current density decreases exponentially with the barrier thickness as the halfwidth of the resonance Eq. (16).

While the absolute peak-current densities resulting from simulations are in good agreement with experimental data, the calculated valley current densities are one or more orders of magnitude lower than the experimental ones. For AlAs/GaAs or AlAs/InGaAs diode structures on GaAs the experimental PVRs at room temperature are in the order of 6. The predicted PVR values from simulations are more than one order of magnitude higher (see Figure 7b and [10]). The reason for this discrepancy is the neglect of scattering effects in the calculation. Scattering effects broaden the resonance in the transmission probability while simultaneously damping it. The peak current density is nearly not sensitive to scattering effects but the valley current and the PVR are very strongly influenced.

An appropriate scattering model is based on the Breit-Wigner generalization of the Lorentzian form of the resonant transmission probability. Within this formalism resonant tunneling in one dimension is studied by Stone *et al.* [3] who derived the total transmission probability in the presence of inelastic scattering for a symmetric structure as:

$$T_{tot}=\frac{\frac{1}{4}\Gamma_0\Gamma}{(W-W_r)^2+\frac{1}{4}\Gamma^2}$$

where Γ_0 is the half width of the resonance in the coherent transmission pro
$\Gamma=\Gamma_0+\Gamma_i$ is the total resonance half width, Γ_i representing the contribution t
ening due to the inelastic scattering. Büttiker [4] has interpreted this total t
probability as a sum of a coherent and sequential transmission probabilities

$$T_{tot}=T_c+T_i$$

In this picture of scattering the fraction of carriers penetrating the structure
$T_c/T_{tot}=\Gamma_0/\Gamma$ and the fraction of carriers traversing the structure se
$T_i/T_{tot}=\Gamma_i/\Gamma$. From these results one can infer that the smaller the elastic
smaller is the amount of scattering needed to make the sequential tunn
dominant. This means that in tunneling diodes with thick barriers (sharp re
spite of a small scattering probability, considerable sequential tunneling c
will be observed. Furthermore, Eq. (20) can be interpreted as a folding of
transmission probability (Eq. (20)) with $\Gamma_i = 0$) with a normalized Loren
width Γ_i. In current density calculations this mechanism conserves the peak
sity but affects the valley current very strongly resulting in lower PVR va
kind of treatment of I - V curves the effect of scattering is used as a fitting
determine the resonance broadening at room temperature. For a typical RT
AlAs barriers and a 5 nm GaAs quantum well a resonance halfwidth of ab
room temperature was found (see [5]).

From the theoretical point of view this treatment of scattering is not
Therefore a more complex approach is needed. In an enhanced calculation
rium Green-function theory is the base of the calculations in which s
charging, incoherent and inelastic scattering, and the band structure is con
et al. [6] have developed a complex simulation package in which most o
effects are taken into account. A real-space tight binding formulation prov
rate synthesis of heterostructures on an atomic scale. It implies the con
inter-valley and inter-band transitions and gives a sophisticated descriptio
in the gap-region ("band-wrapping"). This approach was the base for
device simulation package NEMO (NanoElectronic MOdeling) that sim
variety of quantum devices, including RTDs, HEMTs, HBTs, superlattic
diodes.

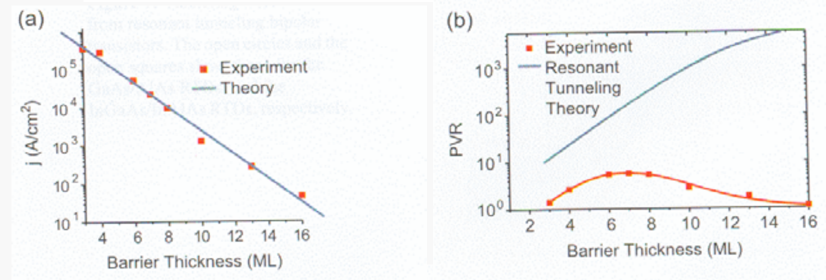

Figure 7: Comparison between theory according to Eq.(19) and experiment for a GaAs resonant tunneling diode (a) peak current density, (b) PVR.

Resonant Tunneling Diode (RTD) III

Figure 8: PVR of an AlAs/GaAs double barrier structure as a function of growth temperature (left). The optimum growth temperature of about 600 °C corresponds to the best quality of the interface in the HRTEM picture (right).

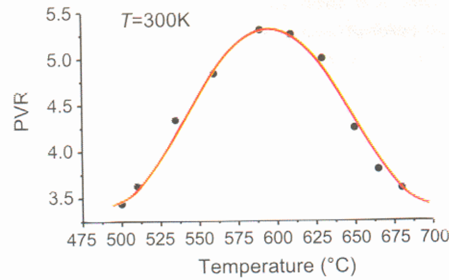

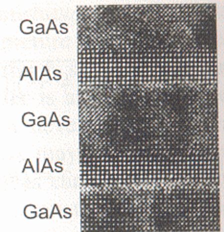

Dependence on fabrication parameters (interface issues)

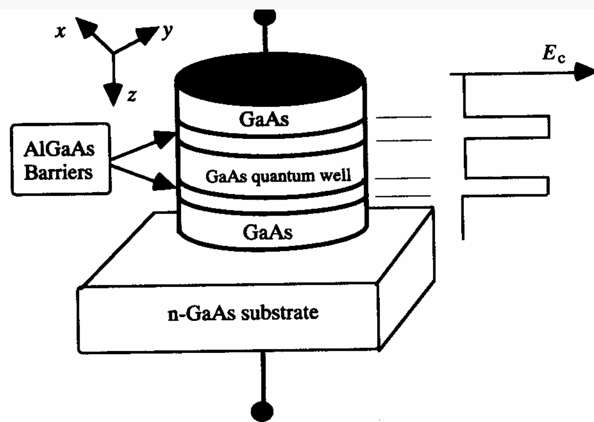

Fig. 6.1.1. Resonant tunneling device. A GaAs layer a few nanometers thick is sandwiched between two AlGaAs barrier layers of similar thickness. Adapted with permission from Fig. 2 of F. Capasso and S. Datta (1990), *Physics Today*, **43**, 74.

Example of RTD structure

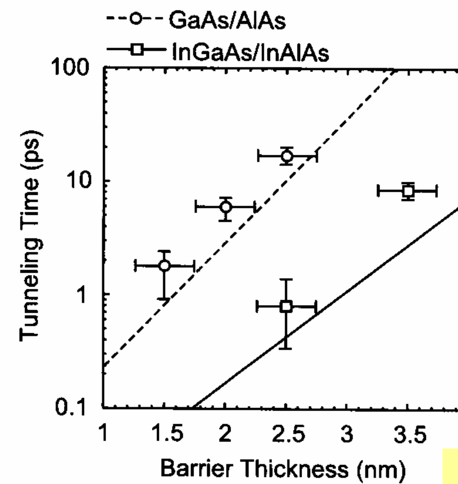

Huge speed!

Figure 9: Tunneling time obtained from resonant tunneling bipolar transistors. The open circles and the open squares show those for the GaAs/AlAs RTDs, and the InGaAs/InAlAs RTDs, respectively.

Conclusions

✓ Transport properties (conductivity) is strongly affected by dimensionality

✓ Lower dimensionality implies a different functional dependence of DOS on the energy

✓ Quantum confinement effects may arise when considering nanostructures with size comparable to the de Broglie wavelength

✓ Quantum Hall Effect (2DEG + magnetic field) demonstrated quantized resistance

✓ Similar quantization effects (but for factor 2!) is observed also in 1DEG systems (e.g., electron waveguides)

✓ 0DEG features (quantum dots) can be used to achieve tunneling ruled by peculiar phenomena (e.g., Coulomb blockade)

✓ 0DEG-based devices exhibit the potential for single electron manipulation

✓ Tunneling with resonant features exploitable for novel devices